REPUBLIC OF TURKIYE
ADANA ALPARSLAN TURKES SCIENCE AND TECHNOLOGY UNIVERSITY

INSTITUTE OF GRADUATE EDUCATION
DEPARTMENT OF MECHANICAL ENGINEERING

INVESTIGATION OF IMPACTS OF GRAPHENE-DOPED FUEL BLENDS ON GREENHOUSE GAS EMISSIONS

ALİ CAN MERT

MASTER OF SCIENCE

ADANA 2024

REPUBLIC OF TURKIYE
ADANA ALPARSLAN TURKES SCIENCE AND TECHNOLOGY UNIVERSITY

INSTITUTE OF GRADUATE EDUCATION
DEPARTMENT OF MECHANICAL ENGINEERING

INVESTIGATION OF IMPACTS OF GRAPHENE-DOPED FUEL BLENDS ON GREENHOUSE GAS EMISSIONS

ALİ CAN MERT

MASTER OF SCIENCE

SUPERVISOR
ASSOCIATE PROFESSOR ASLI ABDULVAHITOĞLU

ADANA, 2024

ÖZET

GRAPHEN KATKILI YAKIT KARIŞIMLARININ SERA GAZI EMİSYONLARI ÜZERİNDEKİ ETKİLERİNİN İNCELENMESİ

Ali Can MERT
Yüksek Lisans, Makine Mühendisliği Anabilim Dalı
Danışman: Doçent Dr. Aslı ABDULVAHİTOĞLU
Temmuz 2024, 72 sayfa

Sürdürülebilir enerji kaynakları arayışı, iklim değişikliğini hafifletme ve çevresel bozulmayı azaltma ihtiyacı nedeniyle onlarca yıldır küresel bir endişe kaynağı olmuştur. Sanayi devriminden bu yana, kömür, petrol ve doğal gaz gibi fosil yakıtlara olan bağımlılık, modern medeniyetin enerji tüketiminin temel taşı olmuştur. Ancak, bu fosil yakıtların yanması, atmosfere önemli miktarda sera gazı (GHG), öncelikle karbondioksit (CO_2), metan (CH_4) ve azot oksit (N_2O) salmaktadır ve bu da küresel ısınma ve iklim değişikliğine katkıda bulunmaktadır. Enerji, günümüzde insanlar için en önemli ihtiyaçlardan biridir. Günümüzde fosil yakıtların piyasaya girmesi ve zararlarının ortaya çıkması nedeniyle, inşaat yeni ve daha çevre dostu bir yakıt kaynağına yönlendirilmiştir. Bunlardan biri, nano partiküllerden oluşan grafen ve grafen oksittir. Bu ışıldayan grafen ve grafen oksit ilaveli yakıtlar üzerinde çalışmalar yapılmaktadır. Bu çalışmada, çeşitli grafen oranları ile karıştırılmış optimum yakıt karışımına karar vermek için yedi farklı MCDM yöntemi kullanılmıştır.

Anahtar Kelimeler: Grafen,Grafen oksit, Nano parçacık

ABSTRACT

INVESTIGATION OF IMPACTS OF GRAPHENE-DOPED FUEL BLENDS ON GREENHOUSE GAS EMISSIONS

Ali Can MERT

M.Sc., Department of Mechanical Engineering
Supervisor: Assoc. Prof. Aslı ABDULVAHITOGLU

JULY 2024, 72 pages

The quest for sustainable energy sources has been a pressing global concern for decades, driven by the need to mitigate climate change and reduce environmental degradation. Since the industrial revolution, reliance on fossil fuels such as coal, oil, and natural gas has been the cornerstone of modern civilization's energy consumption. However, the combustion of these fossil fuels releases significant quantities of greenhouse gases (GHGs), primarily carbon dioxide (CO_2), methane (CH_4), and nitrous oxide (N_2O), into the atmosphere, contributing to global warming and climate change.Energy is one of the most important needs for people today. Nowadays, due to the introduction of fossil fuels into the market and their damages, construction has been directed to a new and more environmentally friendly fuel source. One of these is graphene and graphene oxide consisting of nano particles. Studies on these glowing graphene and graphene oxide added fuels are taken. In this study, seven different MCDM method was used in order to decide the optimum fuel blend mixed with various graphene ratios.

Keywords: Graphene,Graphene oxide,Nano particle

Dedication

Bu çalışmada değerli bilgi ve tecrübelerinden yararlandığım danışman hocam Doç.Dr. Aslı ABDULVAHİTOĞLU'na tüm içtenliğimle teşekür ederim. Bilgi birikiminiz, özveriniz ve samimi rehberliğiniz sayesinde, öğrenme sürecimde büyük ilerlemeler kaydettim. Sadece akademik değil, aynı zamanda insan olarakta sizden çok şey öğrendim. Değerli zamanınızı bana ayırdığınız için size çok teşekkür ederim. Bu çalışmamda emeği geçen tüm Adana Alparslan Türkeş Bilim ve Teknoloji Üniversitesi çalışanlarına sonsuz hürmetlerimi sunarım. Aynı zamanda bu süreçte bana maddi manevi desteğini eksik etmeyen aileme çok minnettarım.

TABLE OF CONTENTS

LIST OF FIGURES

LIST OF TABLES

LIST OF ABBREVIATIONS

COF: Coefficient Of Friction

SEM: Scannig Electron Microscope

DLS: Dynamic Light Scattering

UV-Vis: Ultraviolet-Visible spectrometer

SFC: Specific Fuel Consuption

UHC: Unburned-Hydrocarbon

OF: Oxygenated Fuels

BTE: Brake Thermal Efficiency

BSFC: Brake Specific Fuel Consumption

EGT: Exhaust Gas Temperature

ID: Ignition Delay

EVC: Exhaust Valve Closing

IVC: Intake Valve Closing

BDC: Bottom Dead Center

EVO: Exhaust Valve Open

IVO: Intake Valve Open

B20: Diesel Biodiesel Mixture

GO: Graphene Oxide

GHD: Greenhouse gas

CVD: Chemical Vapor Depositiont

GO: Graphene Oxide

GtF:Graphen Fluoride

RGO: Reduced Graphene Oxide

HHV: Higher Heating Value

LIST OF SYMBOLS

CO: Carbonmonoxide

CO_2: Carbondioxide

SiC: Slicon Carbide

HC: Hydrogen Chloride

CeO_2: Cerium Oxide

C: Carbon

H: Hydrogen

O: Oxygen

Si: Silicon

Ge: Germanium

Ga: Gallium

Al: Aluminum

N: Nitrogen

Bi: Bismuth

UV: Ultraviolet

IR: Infrared

GaAs: Gallium Arsenide

GaBi: Gallium Bismide

GaN: Gallium Nitride

AlAs: Alluminium Arsenide

ZnS: Zinc Sulphide

NOX: Nitrogen oxide emissi

1.INTRODUCTION

The quest for sustainable energy sources has been a pressing global concern for decades, driven by the need to mitigate climate change and reduce environmental degradation. Since the industrial revolution, reliance on fossil fuels such as coal, oil, and natural gas has been the cornerstone of modern civilization's energy consumption. However, the combustion of these fossil fuels releases significant quantities of greenhouse gases (GHGs), primarily carbon dioxide (CO_2), methane (CH_4), and nitrous oxide (N_2O), into the atmosphere, contributing to global warming and climate change.

In response to these challenges, researchers and policymakers alike have been exploring alternative energy sources and technologies to transition towards a low-carbon economy. One such promising avenue is the utilization of graphene, a two-dimensional allotrope of carbon with remarkable properties, in fuel technology. Graphene's exceptional conductivity, mechanical strength, and high surface area make it an ideal candidate for enhancing the performance of various energy systems, including fuel cells, batteries, and, more recently, fuel blends.

One of the indispensable elements for humanity is energy. It forms the basis of economic development. As the world population increases every year, the demand for energy also increases. Fossil fuels can cause negative effects on human health and the environment.

It can produce relatively high amounts of pollutants (hazardous pollutants such as hydrocarbon, carbon dioxide, carbon monoxide, sulfur dioxide, particulate matter, and nitrogen oxides) and greenhouse gas (GHG) emissions. These hazardous pollutants have been proven to be harmful to human health. It also causes global warming. As a result, it leads to various disasters such as drought and flood. Because petroleum-based fuels are limited and the emissions they release are high, researchers have generally turned to examining alternative fuels. Given the impacts of burning fossil fuels, researchers around the world are focusing their attention on the sustainable development of renewable and clean energy sources.

Bioethanol and biodiesel are considered primary alternative energy sources to replace non-renewable and conventional fossil fuels. Renewable oil-rich feedstocks, including animal fats, vegetable oil and algae-derived mixture of fatty acid methyl esters, are known as biodiesel. One of the most striking advantages of biodiesel, which replaces non-renewable fuels as a renewable resource, improve engine performance. In addition, other advantages that make it attractive to use biodiesel fuel in engines are; less cost, less exhaust emissions and ease of supply of raw materials.

Nowadays, new additives are added to biodiesel fuels used as alternative fuels to reduce emission values and increase engine performance. These additives are currently mostly nanoparticles that emerge with the development of technology. The mixture of these particles with diesel/biodiesel fuels provides better engine performance and less NO_x ,CO,CO_2 etc. It is thought that emission gases can be reduced. And with the continuous development of

technology, studies are being carried out on these. It has been revealed by some studies that by using these particles, engine efficiency will increase and friction will be minimized. One of the leading ones of these nano particles is graphene and graphene oxide. With the use of these parts, in-engine mechanics It has been stated by scientists as a result of some experiments that friction will be less, thermal efficiency and engine life will increase. This additive can be used in diesel/biodiesel etc. It is thought that the emission values will decrease as a result of using fuels in a diesel engine, and as a natural result, the damage to the environment will decrease and the greenhouse effect will decrease a little more. It is thought that the production of graphene will make a new contribution to alternative fuels. Graphene is an alternative fuel that can be used in many areas. It is 1000 times stronger than steel. It has a stronger structure. It is anticipated that this substance will be easier to produce with the development of technology and that this substance will be used in more areas.

In this study, studies on the use of graphene as an additive in diesel and biodiesel fuel will be examined. In these studies, the engine performance of this mixture and the emission gases resulting from combustion were examined. The methods used in the studies were followed and how these methods were demonstrated. In the study, 30,60,90 ppm graphene, 0%,10%,20% diesel-biodiesel fuel mixtures were examined. Multi-criteria decision-making method was used to determine which alternative was the best. 8 different methods were used in this method. Fuel mixtures; CO, CO_2, NO_x, Brake power, Density, Kinematic Viscosity, Cetane Number and such criteria were numbered one by one. According to these criteria, the best alternative fuel was determined. The study tried to simplify the processes by finding the best alternative.

1.1.Graphene

The layer of carbon atoms that has a hexagonal honeycomb-shaped carbon arrangement, is single atom high and is two-dimensional, is called graphene. It is the building block of graphite used in the tips of pencils. Graphene sheets come together to form graphite. Graphite is a three-dimensional material while graphene is two-dimensional. This is the main difference between graphite and graphene. The molecular bond length of graphene, that is, the distance between carbon and carbon, is 0.142 nanometers.

1.1.1.Methods of graphene producing

Graphene can be obtained by many different production methods. The prominent ones can be listed as micromechanical separation of graphite layers (Exfoliation), chemical vapor deposition method, reduction of graphene oxide and epitaxial growth.

1.1.1.1.Exfoliation

Graphite is the form of graphene sheets packed together and connected to each other by van der Waals bonds. For this reason, graphene can be obtained from graphite raw material by using high purity graphite and breaking the weak bonds between them. Mechanical or chemical energies can be used to break these weak bonds. The first study on this subject was conducted

by Viculis et al. in 2003. Viculis and his colleagues mixed graphite and potassium in a certain stereometric ratio, processed them at 200 degrees in a neutral atmosphere, and synthesized the KC8 material, in which potassium atoms are located between graphene layers. When this synthesized material was later taken into ethanol, it was observed that the graphene layers separated from each other as a result of the reaction between potassium and ethanol. In 2004, Novoselev and her colleagues succeeded in producing graphene as thin as a few atoms by using high orientation pyrolytic graphite and adhesive tape, separating the graphite into blocks between the tapes, and repeatedly applying the same process to these separated blocks.

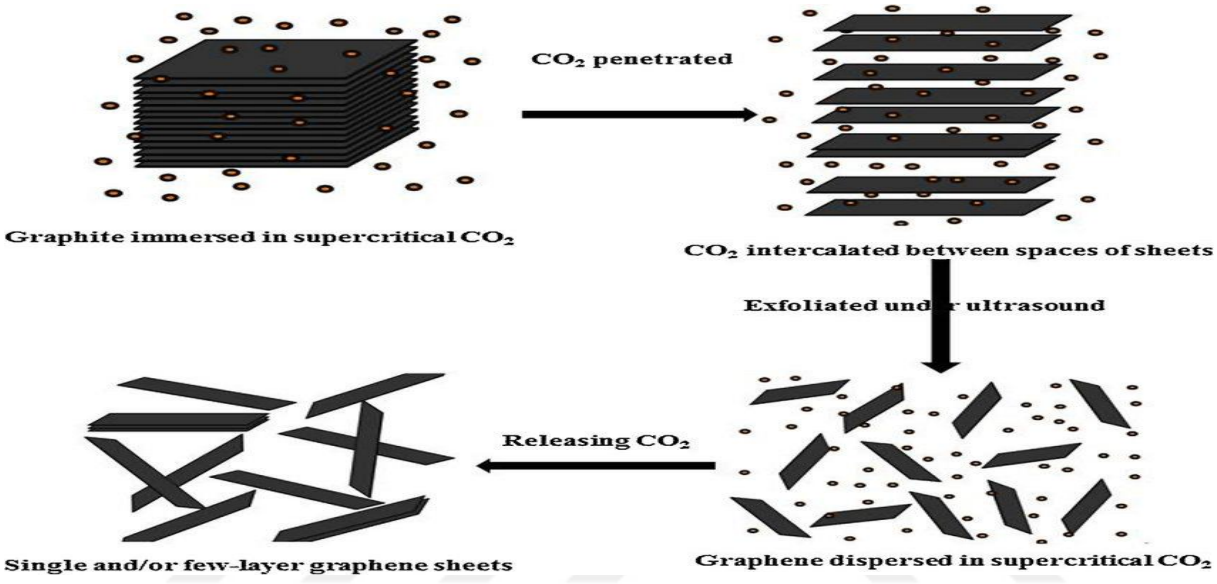

Figure 1.1 Exfoliation (Wang, W.,et al,2014)

1.1.1.2.Chemical vapor deposition method

Although there are many approaches for graphene production, the chemical vapor deposition method (CVD) is accepted as a cheap, efficient, high quality and repeatable production method. It is known that graphene layers obtained by the graphene oxide production and reduction method contain defects. Today, in this method, the deposition process is carried out on transition metals such as Nickel, Palladium, iridium and copper.

The method is basically based on the principle of depositing carbon atoms in the vapor phase on transition metals and then removing them from the surface with a separating agent. Low molecular weight hydrocarbons (such as methane) can be used as carbon sources. The deposition surface to be used must be epitaxially compatible with graphene. In this way, epitaxial growth is achieved.

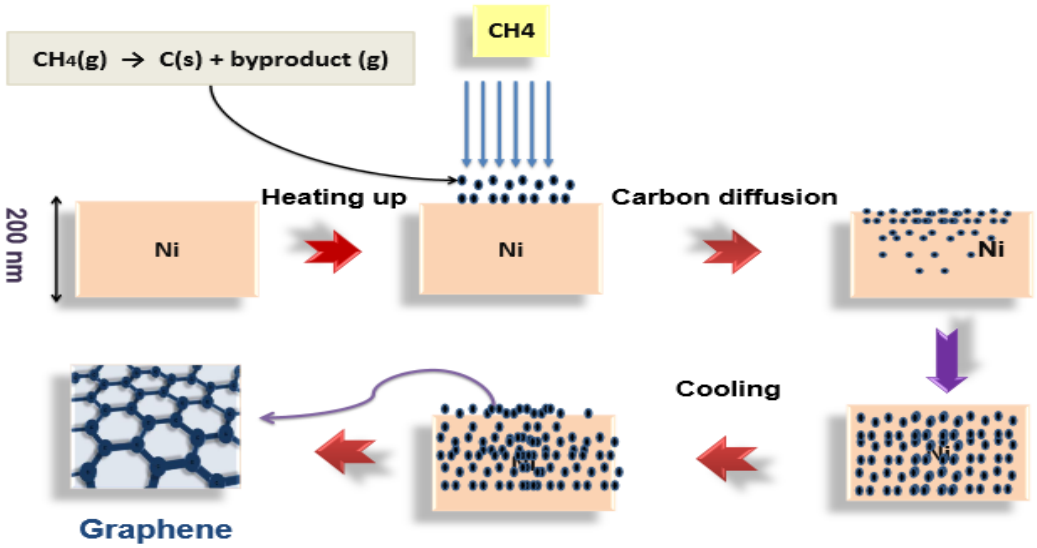

Figure 1.2 Chemical vapor deposition (Al-Shurman,K.,2014)

1.1.1.3.Reduction of graphene oxide

Graphene oxide is a single-layer form of graphite layers separated from each other by oxidation. Graphene oxide contains functional groups with a C:O ratio of less than 3 and typically close to 2. One of the prominent methods for the production of graphene in high quantities is the reduction of graphene oxide produced from graphite by chemical processes using various methods. Two main advantages of this method stand out; these can be summarized as ensuring efficient production by using cheap graphite raw material and preparing stable solutions since the graphite produced is hydrophilic. In 1859, British scientist Brodie discovered that the total weight of graphite increased as a result of his experiment by adding concentrated nitric acid and Potassium Chlorate to graphite powder.

When he determined that the reason for this increase was due to the changes in the chemical structure of graphite and characterized the material he obtained, he determined that the graphite initially contained 96% carbon, but at the end of the experiment, the new composition was approximately 38% oxygen, 2% hydrogen and the remaining 60% carbon. It has been understood that graphite is oxidizable.

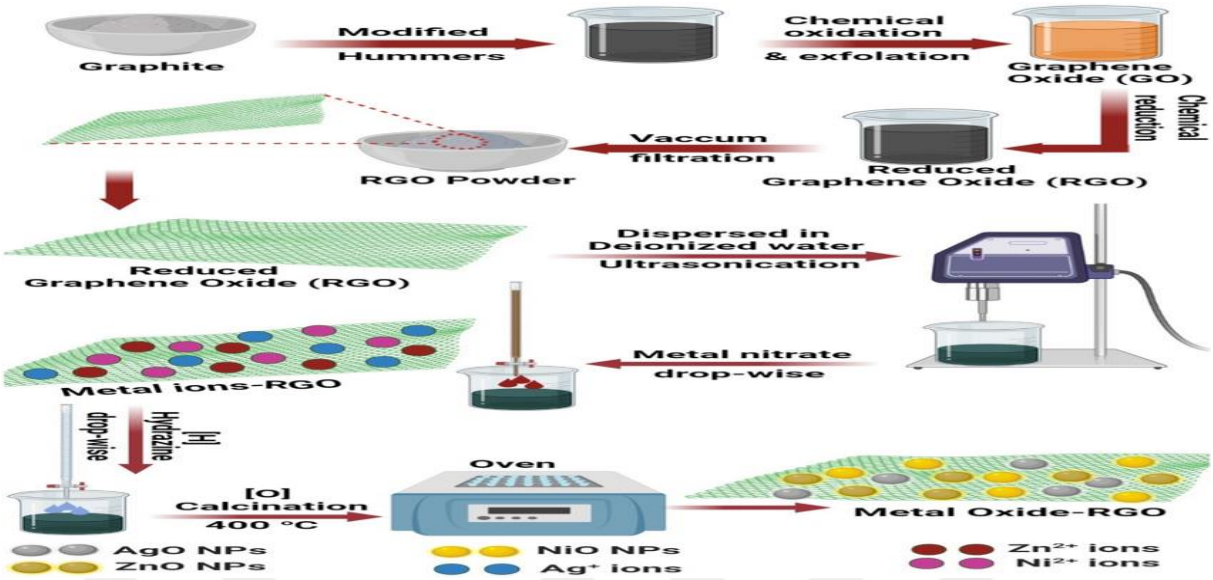

Figure 1.3 Reduction of graphen oxide(Elbasuney, S.,et al,2023)

1.1.1.4.Epitaxial growth

Growing graphene on Silicon Carbide (SiC) is considered as Epitaxial growth.In this method, the SiC layer is heated to a temperature between 1150 and 2000 degrees, depending on the growth conditions. As a result of this heating, silicon desorption occurs and the remaining carbons come together epitaxially to form graphene. Since the carbon source is the SiC layer, new layers form under the first layer and multilayer graphene is obtained. The number of layers of graphene produced depends on the thickness of the SiC layer. The potential problem with this system is that the system is inherently limited. After the first graphene layers are formed, desorbed Si does not find an escape route and may not move away from the layer. This means the end of growth.

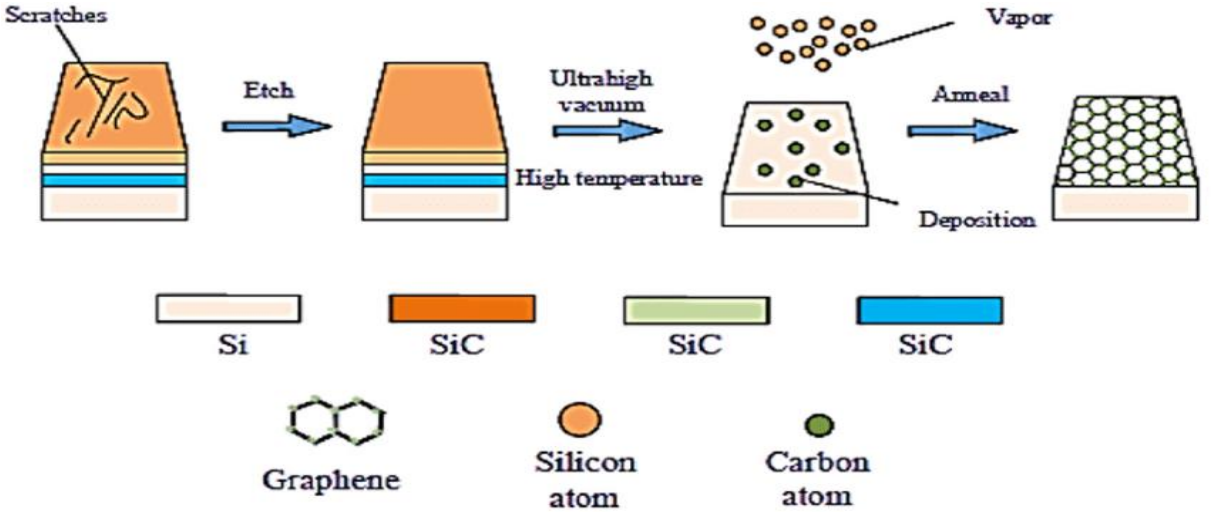

Figure 1.4 Epitaxial growth (Mousavi, S.,et al,2020)

1.1.2. Other methods

1.1.2.1. Axial opening of carbon nanotubes

Single-walled or multi-walled carbon nanotubes can be converted into nanoribbons by axially opening them using various methods. The number of walls of the carbon nanotubes used in this method depends on the number of walls created.

It also determines whether graphene is single-layered or multilayered. The resulting graphene nanomaterial is limited by the diameter of the carbon nanotubes in the transverse direction and by its length in the longitudinal direction.Axial opening of carbon nanotubes can be achieved by physical chemical methods using strong oxidation agents, as well as by physical methods.

1.1.2.2. Arc-discharge Method

One of the current methods to produce multilayer graphene is defined as the arc-discharge method. In this method, direct current is passed through high purity graphite. It has been observed that the buffer gas used during the method directly affects the character of the produced graphene, and different productions with different gas ratios have been carried out in the literature.

Apart from all these, there are many less common methods for the production of graphene, but they are not accepted due to reasons such as low efficiency, increased costs, and the properties of the graphene produced are not at a satisfactory level compared to those produced by basic methods.

Graphene exhibits a wide range of applications across various fields, owing to its exceptional properties. It is particularly noted for its high conductivity, flexibility, and strength-to-weight ratio. Key areas of graphene application include:

- Electronics and Computing: Graphene enables faster and more efficient electronic devices, ranging from transistors to sensors, due to its high conductivity and flexibility.
- Materials Science and Nanotechnology: Graphene has revolutionized materials science with applications in composites for enhanced mechanical strength, water and gas barriers, and various other structural materials.
- Energy Storage and Conversion: Graphene enhances the efficiency of energy storage systems such as solar cells, lithium-ion batteries, and supercapacitors.
- Biomedical Applications: Graphene's biocompatibility and antimicrobial properties make it promising for biosensors, drug delivery systems, biomedical imaging, and tissue engineering.

- Environmental Applications: Graphene is explored in environmental technologies such as water purification, waste management, and removal of environmental pollutants.

The versatility of graphene continues to drive innovation across diverse fields, promising further advancements in technology and sustainable solutions for the future. Utilizing graphene as a fuel additive has emerged as a prominent topic in scientific research. Its potential to enhance fuel efficiency, reduce emissions, and improve combustion dynamics makes it a compelling candidate for addressing challenges in energy and environmental sustainability. Research efforts are actively exploring graphene's role in optimizing fuel performance across various combustion engines, paving the way for cleaner and more efficient energy solutions. A brief seach in web of science core collection with a keyword for Graphene-doped fuel blends (Topic) or Graphene fuel additives (Topic) gives 408 different results. Researchers are actively exploring the potential benefits of incorporating graphene into fuel formulations, likely focusing on enhancing combustion efficiency, reducing emissions, and improving overall engine performance. This wealth of literature underscores the importance and potential of graphene in advancing fuel technologies towards more sustainable and efficient solutions. As it can be seen in the below figures.

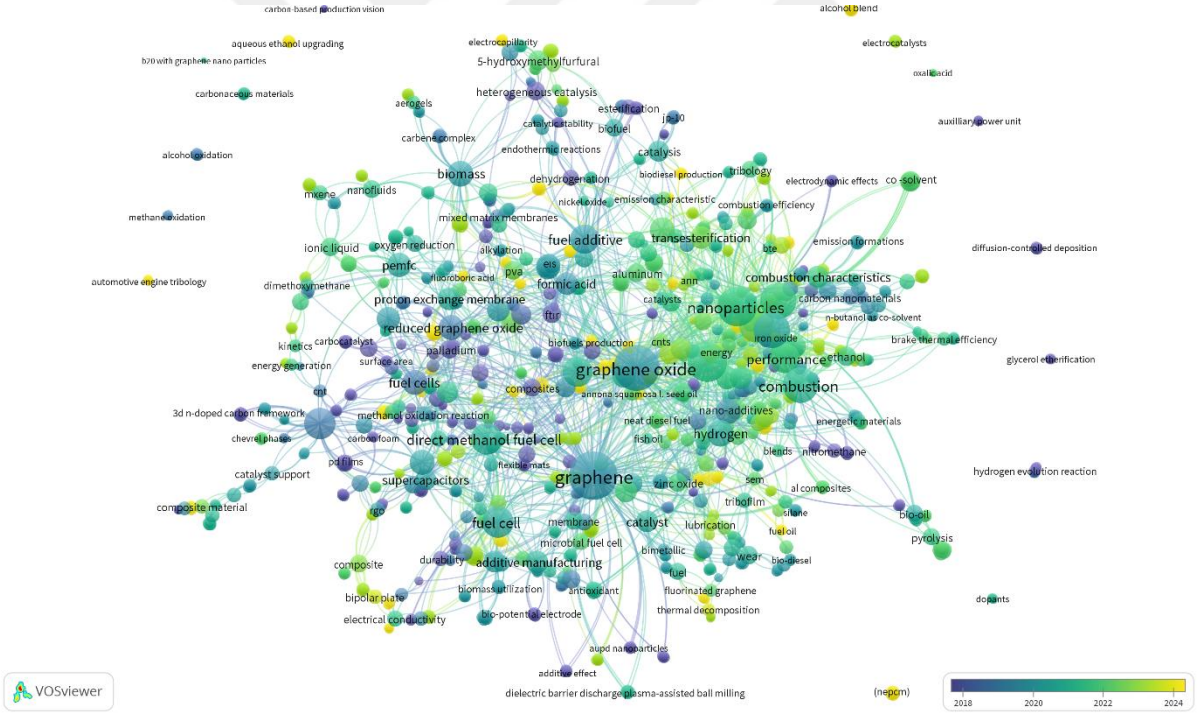

Figure 1.5: Keywords employed to retrieve literature (Created by author)

This figure illustrates the keywords used in the search, highlighting "Graphene-doped fuel blends (Topic)" and "Graphene fuel additives (Topic)" as the primary keywords employed to retrieve relevant literature.

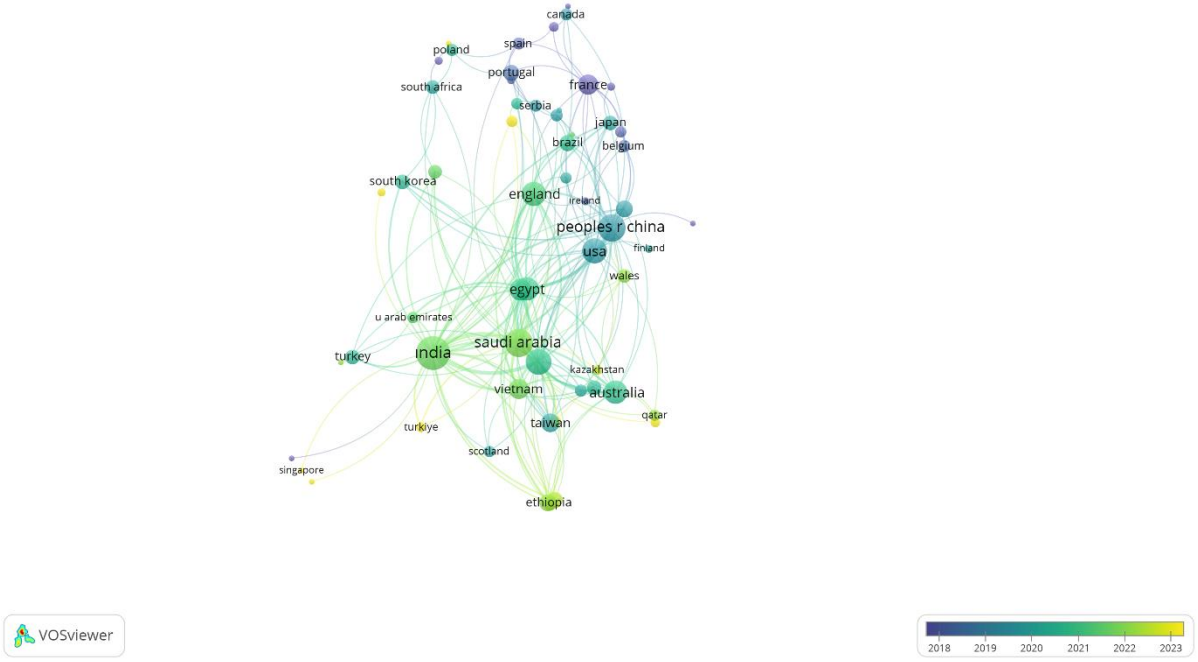

Figure 1.6: Global interest and disturibution of scientific effort (Created by author)

Figure 1.6 displays the countries currently engaged in research within this area, reflecting the global interest and distribution of scientific efforts related to graphene-enhanced fuel technologies.

The development of graphene-doped fuel blends presents an innovative approach to improving the efficiency and environmental impact of conventional fuel combustion. By incorporating graphene into fuel formulations, it is hypothesized that the combustion process can be optimized, resulting in reduced emissions of GHGs and other pollutants. However, despite growing interest in this area, the extent of graphene's impact on greenhouse gas emissions remains poorly understood.

In today's complex and rapidly evolving engineering landscape, decision-making processes are becoming increasingly challenging due to the multitude of criteria that need to be considered simultaneously. Mechanical engineering, in particular, demands rigorous analysis and evaluation of alternatives based on diverse and often conflicting criteria such as cost, performance, reliability, safety, and environmental impact. To address these challenges, Multi-Criteria Decision Making (MCDM) methods have emerged as indispensable tools. This essay explores the necessity of MCDM methods, their applications in mechanical engineering, and specific methods that have proven beneficial in this field.

In mechanical engineering, decision-making scenarios are rarely straightforward. Engineers are frequently faced with complex problems that require balancing multiple objectives and constraints. For instance, when selecting materials for a new product, an engineer must consider factors such as strength, weight, cost, availability, and environmental impact.

Traditional single-criterion decision-making methods fall short in such scenarios, as they cannot adequately capture the trade-offs between different criteria.

MCDM methods address this limitation by providing a structured framework for evaluating and prioritizing alternatives based on multiple criteria. These methods enable engineers to systematically assess all relevant factors, incorporate expert judgments, and derive comprehensive solutions that are aligned with overall project goals and constraints. By doing so, MCDM methods enhance the quality and robustness of engineering decisions, leading to improved outcomes and reduced risks.

A brief seach in web of science core collection with a keyword for MCDM and Engineering search with in topic gives 546 results. The results indicating a robust interest and extensive research in the application of Multi-Criteria Decision-Making (MCDM) in engineering. This broad search encompasses various disciplines within engineering where MCDM methods are utilized to optimize decision-making processes. The significant number of results underscores the versatility and applicability of MCDM in addressing complex engineering challenges and enhancing decision-making frameworks across different domains.

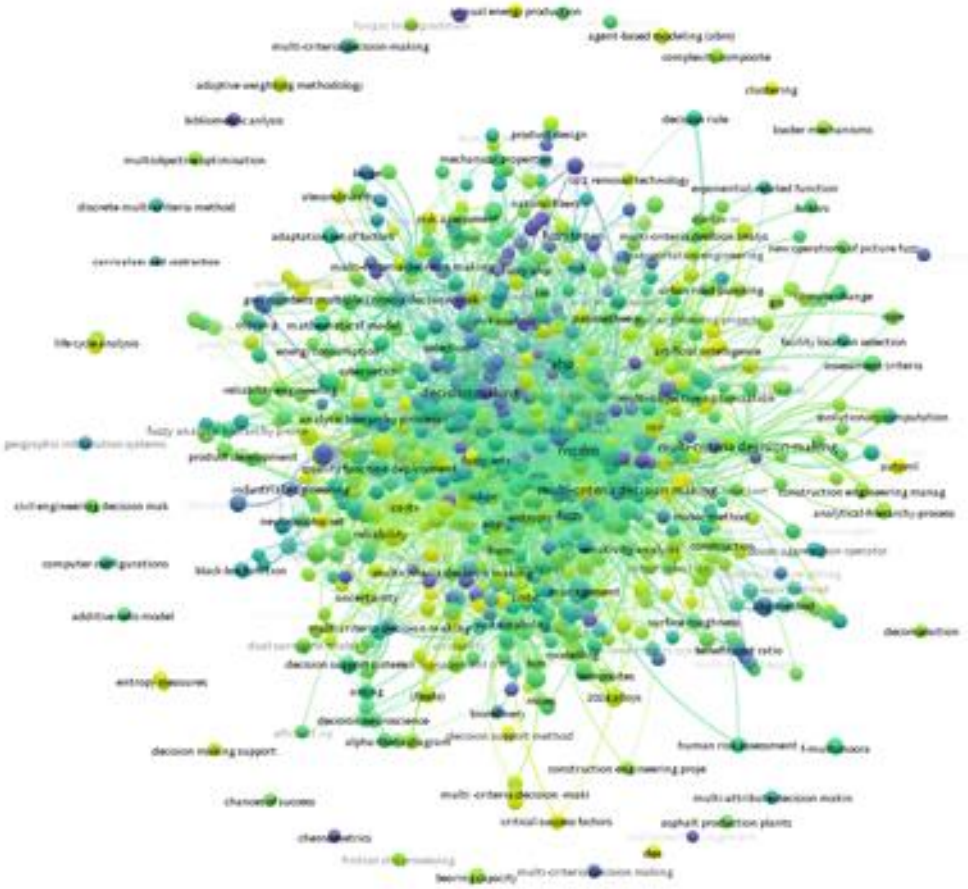

Figure 1.7: Keywords employed to retrieve literature on MCDM (Created by author)

This figure illustrates the keywords used in the search, highlighting "Multicriteria Decision Making (Topic)" and "Engineering" as the primary keywords employed to retrieve relevant literature.

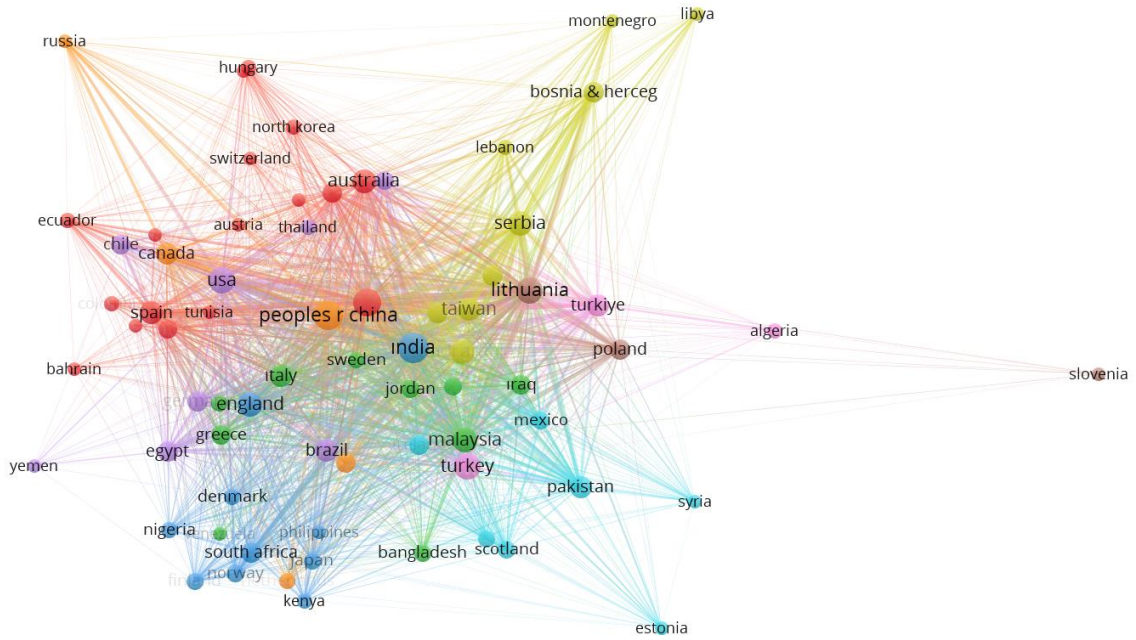

Figure 1.8: Global interest and disturibution of scientific effort (Created by author)

Figure 1.8 displays the countries currently engaged in research within this area, reflecting the global interest and distribution of scientific efforts related to MCDM approach.

MCDM methods find applications in a wide range of mechanical engineering domains, including but not limited to:

- Material Selection: Selecting the appropriate material for a specific application is crucial for the performance and durability of mechanical components. MCDM methods help evaluate different materials based on criteria such as mechanical properties, cost, manufacturability, and environmental impact.
- Design Optimization: During the design phase of mechanical systems, engineers must consider various performance metrics such as efficiency, reliability, and cost. MCDM methods facilitate the identification of optimal design solutions by evaluating trade-offs among these metrics.
- Supplier Selection: Choosing the right supplier is essential for ensuring the quality and reliability of mechanical components. MCDM methods assist in evaluating suppliers based on criteria such as cost, quality, delivery performance, and sustainability practices.
- Manufacturing Process Selection: Selecting the most suitable manufacturing process involves considering factors such as production cost, lead time, quality, and flexibility.

MCDM methods enable a systematic comparison of alternative processes to identify the best option.

- Maintenance and Reliability: In maintenance planning, engineers must prioritize tasks based on factors like criticality, cost, downtime, and safety. MCDM methods help in developing effective maintenance strategies that balance these considerations.
- Project Management: In project management, MCDM methods are used to prioritize projects, allocate resources, and manage risks by evaluating multiple project objectives and constraints.

There are several MCDM methods are widely used in literature, such as TOPSIS, COPRAS, MAUT, MOOSRA etc.

The existing literature on graphene-doped fuel blends lacks comprehensive studies that apply Multi-Criteria Decision Making (MCDM) approaches to assess their impact on greenhouse gas emissions. While previous research has identified key criteria for evaluating fuel additives, such as combustion efficiency and emissions reduction, there is a lack of consensus on the most effective MCDM methodology for integrating these criteria. Additionally, there is limited empirical data on the environmental performance of graphene-doped fuel blends under real-world operating conditions. Addressing this gap is crucial for informing sustainable fuel development strategies and mitigating the environmental impact of transportation.

The remainder of this thesis is organized as follows: Chapter 2 provides a comprehensive literature review on graphene-doped fuel blends and their effects on greenhouse gas emissions and MCDM approach. Chapter 3 provides brief explanation abot combustion in an internal combustion engine. Chapter 4 outlines the methodology employed for conducting the MCDM methods. Chapter 5 presents the results of the calculations, followed by a discussion of the findings. Finally, Chapter 6 concludes the thesis by summarizing the main findings, discussing their implications, and suggesting avenues for future research.

2. LITERATURE REVIEW

Nowadays, there are many studies on fuel mixtures with nanoparticles additives. Graphene additive fuel mixtures are one of them. Investigations are carried out on the engine performance and emission properties of graphene. In this section, studies on the use of nanoparticles such as graphene as additives are mentioned and theoretical studies on this are summarized.

Sajeevan and Sajith conducted an experimental study on the effects of cerium oxide (CeO_2) nanoparticles in diesel fuel. They varied the nanoparticle concentration from 5 to 40 ppm and tested using a single-cylinder, 4-stroke, water-cooled diesel engine. Their findings showed that at higher engine loads, efficiency improved by up to 5%, attributed to cerium oxide nanoparticles acting as oxygen buffers. This facilitated more complete combustion by releasing and storing oxygen due to partial pressure. They also observed significant reductions in hydrocarbon (HC) and nitrogen oxide (NO_X) emissions, which increased with higher nanoparticle concentrations in the fuel. The study determined that the optimal nanoparticle concentration for minimizing emissions was 35 ppm. (Sajeevan, A.,Sajith,V.,2013)

Karthikeyan and Prathima investigated converting Botryococcus braunii algal oil into methyl ester and adding cerium oxide nanoparticles at 50 ppm, 75 ppm, and 100 ppm. They tested the blend in a single-cylinder engine and found that while CO_2 and NO_X emissions increased, CO and HC emissions decreased when using diesel biodiesel (B20) with cerium oxide nanoparticles. (Karthikeyan,S., Prathima A., 2017).

Ranaware and Satpute studied enhancing diesel engine performance and emissions using cerium oxide nanoparticles and hydrous iron liquid additives in diesel fuel. They found that cerium oxide acts as an oxygen-donating catalyst, improving CO oxidation and reducing NO_X emissions. Their research showed that CeO_2 nanoparticles lower HC emissions by aiding combustion of carbon deposits in engine cylinders at wall temperatures. They noted important gains in thermal efficiency and decreases in specific costs, up to 100,000 times and 500 times respectively compared to conventional diesel. Despite increased CO emissions, NO_X emissions were lower than with standard diesel fuel. (Ranaware, A., Satpute S., 2013).

Vellayan studied the impact of cerium oxide nanoparticle additives in soybean biodiesel emulsified in water using a single-cylinder diesel engine. They tested two formulations: SB5W100CeO_2 and SB10W100CeO_2, with 100 ppm cerium oxide nanoparticles and 5% and

10% water by volume in soybean biodiesel, respectively. The research showed that adding cerium oxide nanoparticles increased maximum cylinder pressure and heat release of pure soybean biodiesel, while decreasing peak combustion parameters (Vellayan S., 2020).

An and Ark blended waste cooking oil biodiesel with diesel from 5% to 100%, finding that higher biodiesel concentrations like B100 improved combustion efficiency due to oxygen content, achieving up to 38.1% thermal efficiency. However, specific fuel consumption rose significantly with higher biodiesel ratios, showing a 34.4% increase for B100. They observed minimal hydrocarbon (HC) and carbon monoxide (CO) emissions, credited to biodiesel's lower viscosity and cleaner combustion traits (An, H., et al., 2013).

Muralidharan and Vasudevan studied biodiesel from waste cooking oil blended with diesel (20%, 40%, 60%, and 80%) in a single-cylinder engine with flexible compression ratio. Increasing compression ratio enhanced thermal efficiency up to 31.48%, comparable to standard diesel at high ratios. Specific fuel consumption decreased with higher biodiesel content; B40 had higher energy content than B60 and B80, but less than B20 and regular diesel. At compression ratio 21, B40's specific fuel consumption was 0.259 kg/kWh. The blends reduced HC, CO_2, and CO emissions, but increased NO_X emissions (Muralidharan, K.,Vasudevan, D.,2011).

Chen Zhe, Liu Yuhong, and Luo Jianbin highlighted the importance of lubricant additives and the environmental issues associated with current options. They proposed graphene oxide (GO) as a promising, environmentally friendly additive for hydrocarbon-based oils. Their study showed that adding few-layer GO sheets decreased friction coefficient and wear while expanding the lubricant's temperature range, especially under higher sliding speeds. The optimal concentration of GO was found to be 0.5 wt% (Chen, Z., et al., 2016).

Aram Heidari-Maleni, Tarohom Mesri, and Gurdoshmian studied the effects of Graphene Quantum Dot (GQD) nanoparticles in an ethanol-biodiesel blend (B10) on a diesel engine. GQD nanoparticles at 30 ppm were added to each fuel blend, tested at engine speeds of 1800 rpm, 2100 rpm, and 2400 rpm. The study measured engine power, torque, specific fuel consumption (SFC), and emissions (CO, CO_2, UHC, NO_x). Despite a decrease in power and torque, the research suggested potential benefits of using GQD nanoparticles as additives in improving engine performance and emissions (Heidari-Maleni, A., et al., 2020).

Matesh Agharkar, Sachin Kochrekar, Slah Hidauri, and Musibou Azcez discussed graphene's significant impact on materials science, emphasizing its synthesis methods, particularly the top-down approach from graphite. They highlighted the reduction of graphene oxide as a critical step, traditionally done with strong chemical agents like $NaBH_4$ and hydrazine hydrate. The review focused on environmentally friendly methods for reducing graphene oxide, exploring biomolecules, microorganisms, and plant extracts as natural alternatives (Agharkar, et al., 2014).

Josphat Phiri, Patrick Cane, and Thad C. Maloney studied liquid phase exfoliation methods, emphasizing their cost-effectiveness and scalability. They investigated using graphene as a nanofiller in polymer composites to improve electrical, mechanical, and thermal properties. The study provides valuable insights into the broad applications of graphene in polymer composites (Phiri, J., et al., 2017).

Anindya Nag, Arkadeep Mitra, and Subhas Chandra Mukhopadhyay conducted a comprehensive review of current graphene research, emphasizing its preparation methods, physicochemical characteristics, and utilization as electrodes in sensors. Graphene's outstanding electrical, mechanical, and thermal properties underscore its suitability for sensor applications. The review systematically evaluated sensor performance across different types, synthesizing pivotal insights from multiple research endeavors. Furthermore, the study addressed the persistent challenges in graphene-based sensor technology and proposed prospective solutions (Nag, A., et al., 2018).

S.S. Hoseini, G. Najafi, B. Ghobadian, and M.T. Ebadi studied the physicochemical properties of three biodiesel feedstocks and their performance in diesel engines when blended with graphene oxide (GO) nanoparticles. They evaluated primrose, tree of heaven fruit, and camelina as potential biodiesel sources in Iran, finding camelina oilseeds to have superior properties such as lower viscosity. The research highlighted GO nanoparticles as beneficial additives for improving the quality of biodiesel fuels in Iran (Hoseini, S.S., et al., 2020).

Aman Singh Rajpoot, Tushar Choudhary, H. Chelleadurai, and Norendra Kumar Pasel studied a 4-stroke, single-cylinder CI engine using second-generation Jatropha biodiesel blended with 100 ppm graphene nanoparticles. They categorized the blends by biodiesel and nanoparticle ratios and analyzed engine performance parameters. Results indicated that graphene nanoparticles improved thermal efficiency, reduced fuel consumption, smoke opacity,

and particulate matter emissions, enhancing overall engine efficiency (Rajpoot, A. S., et al., 2023).

Jana and colleagues explored the eco-friendly reduction of graphene oxide (GO) using drained water obtained from soaked mung beans (Phaseolus aureus L.). They highlighted this drained water as a sustainable reducing agent due to its biocatalyst and phytic acid contents. In their approach, mung beans were soaked overnight, and the resulting drained water was collected. This water was then mixed with a GO suspension, and the reduction reaction was conducted under continuous stirring for 24 hours at room temperature (30±2°C). The study verified the efficient reduction of GO and demonstrated favorable electrochemical charge-discharge cyclic stability (Jana, et al., 2014).

Haghighi and Tabrizi employed rose water as a green reducing and stabilizing agent to synthesize reduced graphene oxide nanosheets (RGONs) from exfoliated graphite oxide. The reduction process occurred in a Teflon-lined autoclave at 95°C for 5 hours. X-ray diffraction (XRD) analysis confirmed the removal of oxygen-containing groups, while atomic force microscopy (AFM) and Raman spectroscopy revealed the formation of monolayer RGONs (Haghighi, et al., 2013).

Gurunathan investigated using Ginkgo biloba leaf extract as a natural reducing agent to synthesize graphene. By boiling Ginkgo biloba leaves and adding them to a graphene oxide (GO) solution, they conducted the reduction reaction at 30°C for 12 and 24 hours. Various characterization techniques confirmed the formation of graphene, revealing particles with an average size of about 1400 nm (Gurunathan, S., et al., 2014).

Suresh and colleagues utilized cinnamon extract to reduce graphene oxide (GO) into reduced graphene oxide (RGO). Through refluxing the cinnamon extract with GO at 100°C for 5 hours and subsequently mixing and refluxing the GO suspension for 45 minutes, they achieved efficient reduction, producing few-layered graphene sheets (RGO). The study demonstrated RGO's capability to effectively remove MG and MB dyes without UV or sunlight exposure, highlighting cinnamon extract as a green and effective alternative for GO reduction due to its antioxidant properties (Suresh, D., et al., 2015).

Kuila employed carrot slices in an aqueous solution to reduce graphene oxide (GO) sheets effectively. After soaking the carrot roots at room temperature, they mixed the resulting solution

with a GO dispersion and stirred it for 48 hours. Through transmission electron microscopy (TEM) and atomic force microscopy (AFM), they confirmed the formation of few-layer graphene. Fourier-transform infrared spectroscopy (FTIR) and X-ray photoelectron spectroscopy (XPS) provided evidence of reduced oxygen functionalities on the GO surface, demonstrating the efficacy of carrots as a green reducing agent for GO (Kuila, T.,et al.,2012).

Sunil Jayantha Hettiarachchi and colleagues explored the use of 2D nanocomposites combining Al2O3 and graphene as additives for coconut oil, focusing on their tribological properties. Characterization of the nanocomposite revealed fine particle sizes (< 10 nm), spherical/laminar morphology, and significant sp2 domain content, ensuring stable dispersion as a nanofluid. Their study utilized various analytical techniques to understand friction and wear mechanisms. Optimizing these nanocomposites in coconut oil formulations led to notable reductions in friction coefficient (28%), specific fuel consumption (8%), and emissions of CO, SO2, and NOx, highlighting their potential to enhance fuel efficiency and reduce environmental impact (Hettiarachchi, S.,et al.,2023).

Yue Jiang and colleagues studied the use of boron (B) as a fuel and investigated how graphene oxide (GO) and graphene fluoride (GtF) additives enhance its performance. Their research compared various blends in laser ignition experiments, finding that B/GO/GtF had the shortest ignition delay time, longest burning duration, and highest BO2 emissions. These additives facilitate heat and gas release, improving boron combustion efficiency. The study suggests functionalized graphene materials could significantly enhance the efficiency of energetic materials like metals (Jiang, Y.,et al., 2020).

Vikas Sharma and colleagues studied the impact of blending few-layered graphene and graphite nanoparticles with biodiesel derived from waste cooking oil. They assessed how these additives affected combustion characteristics and engine emissions compared to biodiesel and diesel fuels. By incorporating these nanoparticles into the fuel mixture, they observed a reduction in NO_x emissions by 0.7–5% compared to pure diesel. This research highlights the potential of graphene-based nanoparticle additives to improve biodiesel combustion properties and decrease NO_x emissions (Sharma, V.,et al., 2022).

Manzoore Elahi Soudogar and colleagues studied the effects of graphene oxide nanoparticles added to a biodiesel-diesel blend derived from milk foam oil in compression ignition engines. They used ultrasonication to incorporate graphene oxide at concentrations of

20, 40, and 60 parts per million. Their findings showed significant improvements in engine performance and emissions. Specifically, they observed an 11.56% increase in brake thermal efficiency and an 8.34% decrease in brake specific fuel consumption. Emissions of unburnt hydrocarbons, smoke, and carbon monoxide were reduced by 21.68%, 24.88%, and 38.662%, respectively, for the DSOME2040 blend. Oxides of nitrogen emissions decreased by 5.62% for the DSOME(B20) blend. The addition of graphene nanoparticles also improved combustion characteristics, including shorter combustion duration and ignition delay, as well as enhanced peak pressure and heat release rate under maximum load conditions (Soudagar,et al,2019).

Gowtham and Prakash studied the effects of adding graphene oxide (GeO) to CB20 biodiesel-diesel blend in a compression ignition engine. They found that GeO enhanced combustion efficiency and reduced emissions significantly. Key improvements included increased brake thermal efficiency, cylinder pressure, and heat release rate. Additionally, GeO lowered ignition delay, combustion duration, brake specific fuel consumption, and emissions of carbon monoxide, unburned hydrocarbons, and smoke opacity in the nanofuel blend (Gowtham, M.,et al,2020).

In their research, Tarolhom Mesri Gundarhmian and colleagues explored the effects of incorporating multi-walled carbon nanotube (MWCNT-COOH) additives into B5 biodiesel-diesel blends in a CI engine. They used ultrasonication to disperse MWCNTs-COOH nanoparticles at concentrations of 30, 60, and 90 ppm. Engine tests were conducted across different speeds (1800, 2100, and 2400 rpm) under full load conditions. The study evaluated performance metrics such as power and torque, along with specific fuel consumption (SFC), and emissions including CO, CO2, unburned hydrocarbons (UHC), and NOx. Results showed significant improvements in power and torque compared to pure diesel (D100) and B5 blends, with corresponding reductions in SFC (Gundoshmian, T.,et al.,2021).

In M. Anbarsooz's investigation, the combustion properties of nano-enhanced diesel-biodiesel fuels were comprehensively examined. A comprehensive analysis was conducted on recent studies exploring the effects of diverse nanoparticles on fuel characteristics and combustion behaviors in compression ignition (CI) engines. While certain research highlighted a decrease in NOx emissions, others documented a notable rise in NO_x levels. The majority of these studies employed single-cylinder, four-stroke naturally aspirated engines with power

ratings ranging from 3.7 to 5.5 additives in CI engines necessitate additional research (Anbarsooz, M.,2023).

In their research, M.S. Gad and collaborators conducted an extensive analysis of nano-scale particles in blends of diesel and biofuels, exploring their influence on engine performance. Reviewing multiple studies in this area reveals that incorporating nanoparticles into biodiesel blends leads to decreased exhaust emissions and enhanced combustion properties, credited to the robust catalytic capabilities of these particles. Ultimately, this review decisively illustrates that nanoparticle additives provide a powerful approach for improving combustion efficiency, engine performance, and emission profiles in biodiesel-diesel blends. (Gad, M.,et al., 2023).

M.R. Atelge and colleagues investigated the impact of hybrid nano additives, combining graphene nanoplatelets and TiO2, on combustion and emissions in diesel and oxygenated fuels. Their study found that these additives improved combustion metrics like peak pressure and ignition delay across various engine loads. Additionally, emissions analysis revealed reduced emission levels compared to conventional diesel and oxygenated fuels. Overall, the research highlighted the potential of hybrid nano additives to enhance fuel performance and lower emissions in combustion engines (Atelge, M.,et al,2023).

Rıdvan Küçükosman and colleagues conducted a thorough study on nanoparticle-enhanced fuels (NAFs), focusing on atomization, combustion dynamics, and fuel properties. Their research explored how nanoparticles (NPs) influence both the physics and chemistry of combustion in hydrocarbon fuels. They found that NP size and concentration impact combustion physics, while NP composition, catalytic activity, oxygen content, reactivity, and calorific value influence combustion chemistry. Optimal NP concentrations were identified as 0.5 wt% for spray characteristics and a range of 2.0–2.5 wt% for evaporation and combustion properties in NAFs (Kucukosman,R.,et al.,2022).

Ahmet I. El Seesy and colleagues conducted an experimental study to investigate the effects of graphene oxide (GO) nanoparticles on a diesel engine fueled with Jatropha methyl ester (JME). Their research aimed to enhance engine performance and reduce emissions by blending GO with JME in various concentrations. The study utilized a single-cylinder, air-cooled, direct injection four-stroke diesel engine to evaluate performance metrics such as brake thermal efficiency, peak cylinder pressure, and emissions including CO and unburned hydrocarbons (UHC). Results indicated that incorporating GO nanoparticles improved thermal

efficiency by 17% and significantly reduced CO emissions by 60% and UHC emissions by 50% compared to pure JME fuel (EL-Seesy, A.,et al.,2018).

Cihan Bayındırlı and colleagues investigated the effects of adding reduced graphene oxide (rGO) and graphite nanoparticles to cottonseed oil methyl ester biodiesel through transesterification. They explored how these additives influenced fuel properties like viscosity, calorific value, density, and cetane number. Engine performance and emissions were also evaluated, revealing that rGO, with its enhanced conductivity and surface area, significantly improved both efficiency and reduced fuel consumption. The study demonstrated that at full load, nanoparticle-enhanced fuels boosted brake thermal efficiency by up to 17.97% and lowered brake specific fuel consumption by as much as 16.28%. Additionally, increased nanoparticle concentrations correlated with higher cylinder pressures, indicating improved combustion characteristics (Bayindirli,C.,et al.,2023).

In their study, L. Razzag and colleagues explored the effects of graphene oxide (GNP) and dimethyl carbonate (DMC) additives on palm biodiesel blends in a compression ignition engine. They prepared nanofuels by mixing GNPs into biodiesel-DMC combinations at concentrations of 40, 80, and 120 ppm using ultrasonication. Characterization of GNPs was conducted via Scanning Electron Microscopy (SEM) and Fourier Transform Infrared (FTIR), while rheometry assessed the viscosity of the nanofuels. Engine tests demonstrated that the nanofuels significantly reduced the average friction coefficient by 15.05%, 8.68%, and 3.61% for 120 ppm, 80 ppm, and 40 ppm concentrations, respectively, compared to B30 biodiesel. This research underscores the potential of GNP and DMC additives to enhance diesel engine performance and efficiency (Razzaq, L.,et al.,2021).

Umit Agbulut and colleagues investigated the effects of graphene oxide (GO) nanoparticles as additives in biodiesel-diesel blends used in compression ignition (CI) engines. They conducted experiments on a diesel engine at constant speeds of 2400 rpm and varied loads from 3 to 12 Nm. The study compared pure diesel (B0) with biodiesel blend B15 (85% diesel and 15% waste cooking oil), augmented with GO nanoparticles at concentrations of 100 ppm and 500 ppm. Results showed that blending biodiesel with diesel (B15) reduced brake thermal efficiency (BTE) by 2.67% while lowering CO and HC emissions by 7.5% and 8.53%, respectively. However, it increased brake specific fuel consumption (BSFC) by 5.54% and raised NOx emissions by 3.37% compared to pure diesel (B0). The addition of GO

nanoparticles mitigated these negative effects, suggesting their potential to enhance the overall performance of biodiesel blends in CI engines (Agbulut, U.,et al.,2022).

Ahmet I. El-Seesy and Hamdy Hassan conducted a study to evaluate the impact of graphene oxide (GO), nanoplatelet, and n-butanol-multi-walled carbon nanotube additives on diesel engine performance. The engine was tested at a constant speed of 2000 rpm under varying loads, using Jatropha methyl ester blended with n-butanol (JMB40B) and different carbon nanomaterial additives. Results indicated that while JMB40B blends increased peak pressure and specific fuel consumption compared to pure diesel, the addition of carbon nanomaterials significantly enhanced engine efficiency, reducing fuel consumption by 35%. Moreover, emissions of NOx, CO, and unburned hydrocarbons (UHC) were substantially lowered by 45%, 55%, and 50%, respectively, compared to pure JMB40B blends. This study underscores the potential of carbon nanomaterial additives to improve engine performance by reducing fuel consumption and emissions in biodiesel blends (El-Seesy, A.,et al.,2019).

Hosseini and colleagues investigated the impact of graphene oxide (GO) nanoparticles on a diesel engine fueled with B20 blend of Oenothera lamarckiana biodiesel. They studied GO at concentrations of 30, 60, and 90 ppm across various engine loads at 2100 rpm. The study found that incorporating GO nanoparticles led to increased power output and exhaust gas temperature (EGT). This suggests that GO can effectively enhance engine performance when used with biodiesel blends. Further research is recommended to optimize GO concentrations for maximizing efficiency and minimizing emissions in biodiesel-powered engines (Hoseini, S.,et al.,2020)

Ozer Can and Ozgur Cetin investigated the use of graphene oxide (GO) as an additive in engine oil to enhance energy efficiency in diesel engines. Friction tests conducted on a dynamometer demonstrated that GO nanosheets reduced engine torque by up to 6%, resulting in reduced friction losses and an improvement in mechanical efficiency of up to 2.8% at specific engine speeds. The study also found an average enhancement of 2.6% in brake specific fuel consumption (BSFC) and 2.7% in brake thermal efficiency (BTE) across all engine speeds (Can,O.,et al.,2023).

Meysam Eshaghi Pirey and colleagues conducted a study on the combustion characteristics, performance, and emissions of a diesel engine using graphene oxide nanoparticles (GONPs) blended with diesel and waste cooking oil (WCO) biodiesel mixtures.

The engine operated at full load at 1500 rpm. The researchers assessed emissions of CO, CO2, and NOx, as well as brake power (BP), brake thermal efficiency (BTE), and brake specific fuel consumption (BSFC). The findings indicated that GONPs increased NOx and CO2 emissions while reducing CO emissions. The study concludes that GONPs could effectively enhance diesel and WCO biodiesel fuel blends as additives (Pireh, M.,et al.,2022).

Nagappan Murugan and colleagues investigated the effects of nanographene oxide (NGO) additives on palm oil methyl ester (PME) blended with diesel fuel (B50) in a diesel engine. Their study focused on emission and performance parameters at full load conditions. The results showed significant reductions in hydrocarbon, carbon monoxide, and smoke emissions, attributed to NGO's catalytic properties and increased surface area-to-volume ratio. However, there was a slight increase in nitrogen oxide emissions due to higher peak pressure and combustion heat release. Adding 50 and 100 ppm of NGO improved B50 efficiency by up to 0.9% and decreased fuel consumption by 0.03 kg/kW-h compared to pure B50 biodiesel. (Murugan, N.,et al.,2022).

Deluchi examined the environmental impact of greenhouse gas emissions from various transportation fuels, highlighting the critical importance of reducing these emissions through enhanced vehicle efficiency and the adoption of alternative fuel sources. The study underscores the urgency for further research and emphasizes the implementation of effective pricing strategies to incentivize sustainable practices in transportation (Deluchi,M.,et al.,1987).

Qu demonstrated the exceptional performance of nitrogen-doped graphene as an electrode for oxygen reduction in fuel cells, surpassing electrodes based on platinum. The study emphasized nitrogen-doped graphene's superior catalytic activity, stability, and resistance against crossover and poisoning effects. It underscores the potential of graphene and its derivatives as efficient and cost-effective catalysts in various applications (Qu,L.,et al.,2010).

Indrajit Shown focused on enchancing the photocatalytic reduction of CO2 to hyrdocarbon fuels using Cu-nanoparticle decorated graphene oxide unddder visible light demostrating a significant enhancement in ctalytic efficiency comparedto pristine GO (Shown,I.,et al., 2014).

Najaiabadi examined the adverse environmental effects of carbon dioxide emissions from fossil fuels, highlighting graphene's potential in carbon capture, conversion, and its diverse applications in this domain (Najaiabadi,A.,2015).

Haque et al synthesized and optimized nitrogen-doped graphene samples to enhance the oxygen reduction reaction (ORR) and CO_2 uptake. The study demonstrated how nitrogen doping conditions influence catalytic activity and sorption capacity, particularly for applications in fuel cells. The importance of graphitic nitrogen sites in augmenting catalytic activity was emphasized (Haque,E.,et al.,2016).

Ooi investigates the influence of graphite oxide (GO) nanoparticles on diesel fuel combustion, showing significant improvements in combustion efficiency that could lead to cleaner emssiıons and lower fuel combustion (Ooi,J.,et al.,2016).

Hosseini et al. examined the effect of graphene oxide nanoparticles on the performance and emissions of diesel engines when integrated into Ailanthus altissima biodiesel blends. The study revealed enhancements in engine performance and reductions in specific emissions, indicating the potential for environmentally friendly fuels (Hoseini,S.,et al.,2018).

Feng examined the synthesis, characterization, and applications of boron-, sulfur-, and phosphorus-doped graphene for environmental purposes, elucidating the mechanisms behind these applications and outlining future prospects and challenges (Feng,L.,et al.,2020).

Hosseini investigated how graphene oxide nanoparticles affect the performance and emissions of a diesel engine fueled with B20 blends of Oenothera lamarckiana biodiesel. The study showed improvements in power output and exhaust gas temperature (EGT), alongside decreases in carbon monoxide (CO) and unburned hydrocarbons (UHCs) emissions. There was a slight rise in carbon dioxide (CO_2) and nitrogen oxides (NO_x) emissions. Nano-graphene oxide emerged as a potential additive to enhance these biodiesel blends (Hoseini,S.,et.al,2020).

Nair conducted a study on the effects of blending graphene nanoparticles with Karanja biodiesel on engine performance and emissions. The research demonstrated that blends containing nanoparticles performed comparably to diesel, while achieving reductions in emissions such as CO, HC, and NO_x. The B20G75 blend showed the most substantial decrease in emissions, particularly at higher engine loads (Nair,J., et al.,2021).

Ahmed Ammar proposes graphite nanoparticles as a potentially greener alternative to Fe_2O_3 for improving engine performance and reducing emissions, especially NO_x. These nanoparticles are advocated for application in large turbocharged compression ignition (CI) engines (Ahmed,A.,et al.,2020).

Chacko investigates the effects of graphene oxide (GO) and graphene nanoplatelets (GNP) as fuel additives on combustion and emission characteristics of a diesel engine showing reductions in smoke and nitric oxide emissions making both additive for emission control without adverse effects on filtreability and injector wear (Chacko,N.,Jayeseelan,2020).

Heidari Maleni et al explored the use of graphene quantom dot nanoparticles with ethanol-biodiesel blends to enhance diesel engine performance and reduce emissions with the best fuel combination being B1+E6+GQD90 (Heidari-Maleni,A.,et al.,2021).

Bidir examines the influence of graphene nanoparticles on the performance and emissions of biodiesel blends, revealing enhancements in thermal efficiency and reduced NO_x concentrations. However, the study also identifies negative effects on combustion rate and engine performance at higher graphene nanoparticle (GNP) proportions (Bidir, M.,et al.,2023).

Dwivedi et al. conducted a study aimed at optimizing nano-additives for enhancing Battery Thermal Management Systems (BTMS). Their research focused on integrating multiple decision-making methods to prioritize nano-additives that improve heat transfer and mitigate thermal issues in energy storage devices. Among the nano-additives evaluated, graphene and multi-walled carbon nanotubes (MWCNTs) were identified as the most effective options. The study utilized COPRAS, PROMETHEE-II, and VIKOR methods to assess and rank these additives based on their performance criteria. Sensitivity analyses were also conducted to explore variations in parameters affecting risk preferences and alternative rankings, providing comprehensive insights into nano-additive selection for optimizing BTMS (Dwiedi,A.,et al.,2023).

Raj et al. proposed enhancing Phase Change Materials (PCM) thermal conductivity by incorporating a hybrid nanoparticle blend of aluminium oxide (nAl2O3) and Graphene nano Platelets (GnP), combined with fins. Nanoparticle selection involved Multi-Criteria Decision Making (MCDM). Their study compared Differential Scanning Calorimetry (DSC) and the T-history method to evaluate PCM thermophysical properties. Numerical simulations assessed a hybrid nano-PCM composite in a latent heat storage system with tapered fins, demonstrating improved melting rates. This innovation suggests broad applications in industrial and energy sectors due to its enhanced performance capabilities (Krishma,V.,et al.,2024).

Kavimani et al. investigated the impact of Wire Electric Erosion Machining (WEDM) parameters on Material Removal Rate (MRR) and surface roughness (Ra) for a novel Magnesium metal matrix composite. They studied two material factors (reinforcement weight percentage and SiC additive) and three processing parameters (Pulse On Time, Pulse Off Time, Wire Feed Speed) using Taguchi coupled Gray relationship analysis. The research challenged conventional assumptions by examining how increased P-ON influences MRR. Their goal was to optimize parameters to balance MRR and Ra effectively, considering production costs and time constraints (Kavimani,et al.,2019).

Anandan et al. conducted a study comparing the cooling efficiency of graphene nanofluids with dry and pure Minimum Quantity Lubrication (MQL) during the turning of M42 steel. They varied cutting speeds and feed rates across experiments to assess performance under different operational conditions. Using a hybrid Multi-Objective Optimization by Ratio Analysis (MOORA) method combined with Analytic Hierarchy Process (AHP), they determined optimal turning parameters. Key outcomes measured included surface roughness, cutting temperature, tool wear, and chip morphology analyzed with a scanning electron microscope. Results showed graphene nanofluids significantly reduced surface roughness by 91%, tool wear by 95%, and cutting temperature by 82% compared to dry conditions, highlighting their potential environmental benefits in metal machining processes (Anandan,V.,et al.,2021).

Awate and Barve utilized decision models like TOPSIS and Extended PROMETHEE II to select optimal graphene/Al6061 nanocomposites for enhancing the strength and hardness of Al6061 alloy. Through Analytical Hierarchy Process (AHP), they evaluated various graphene-reinforced variants and identified the 10% graphene-reinforced nanocomposite (10G) as the top performer. It exhibited high ultimate tensile strength (279.69 MPa), hardness (93.73 BHN), and proof stress (248.55 MPa), despite its higher material cost (506.81 Rs). The study suggests potential applications in aerospace, automotive, transportation, defense, and manufacturing sectors (Pankaj,P.,et al.,2022).

Khan et al. explored biosynthesized graphene oxide nanofluids for enhancing solar panel efficiency in photovoltaic thermal systems. Their study evaluated nanofluids under varying Direct Normal Irradiance (DNI), finding graphene oxide achieved the highest efficiency at approximately 62%. Multi-Criteria Decision-Making methods like AHP and TOPSIS ranked nanofluids based on criteria including Exergy loss, Surface temperature, Overall efficiency, and

Electrical efficiency. Graphene oxide emerged as the top performer, followed by copper oxide and cerium oxide, while aluminum oxide ranked the lowest (Khan,F.,et al.,2024).

As can be seen, in most of the studies, the effects of graphene-added diesel-biodiesel fuel mixtures on engine performance and emission values have been investigated. Graphene additives at different ppm values were mixed with diesel or biodiesel fuels at 0%, 10%, 20% and the results were examined. It was observed that graphene-added fuel mixtures increased engine performance such as power, torque, etc. and reduced emission values such as NO_x, CO, CO_2. In this study, the most suitable graphene ppm value and biodiesel fuel ratio were tried to be selected by using the multi-criteria decision-making method to select the most suitable alternative. It was aimed to select the best alternative from these by using 6 different multi-criteria decision-making methods.

3. COMBUSTION

The combustion of a diesel engine is characterized by automatic ignition. At the end of the compression cycle, combustible fuel is injected into the hot, compressed cylinder charge, mixed in, and ignited. During the ignition lag (the time between injection and the commencement of autoignition), a number of complex physical and chemical subprocesses occur, including spray generation, vaporization, mixing, and chain branching (first chemical reactions), with no significant energy conversion (Abdulvahitoglu,2009) .

Ignition is determined by the mixture's initial conditions:

• Charge pressure and temperature • Fuel properties (temperature, viscosity, vaporization, and ignition)

• The pressure, timing, injection characteristics, and nozzle geometry affect spray formation, including droplet size, dispersion, and pulse.

• Charge movements.

• Charge composition, including oxygen content and EGR-induced variations in specific thermal capacity.

• Geometry of the combustion chamber.

Autoignition starts in specific areas where the fuel has fully evaporated and has mixed with enough atmospheric oxygen. During this phase, fuel injection often continues, and both combustion and mixture preparation occur at the same time.

The combustible combination of gasoline and air serves as the working fluid of internal combustion engines. The fuel's stored heat energy is released by this fluid, doing useful work in the process. Maximizing work (power production), limiting energy consumption, and minimizing pollutants generated during the work process are worthwhile objectives shared by all heat engine design and development. The principal elements of a reciprocating engine are seen in Figure 3.1.

Diesel engines compress air to extremely high pressures and then inject a little quantity of fuel into this highly compressed air to produce their remarkable performance and efficiency. Because the fuel in these engines separates from the air for a limited amount of time inside the combustion chamber, the combination of air and fuel is said to as heterogeneous. The highly atomized fuel that is injected evaporates due to the heat produced when the air in the cylinder is compressed. After the evaporated fuel reaches its auto-ignition temperature and combines

with the heated ambient air in the combustion chamber, it ignites. The fuel's stored energy is released during the combustion process. The fuel's auto-ignition temperature is contingent upon its molecular makeup.

In engines that use compression ignition, combustion takes place at various periods when the air-fuel ratio and temperature are just right to support the process.

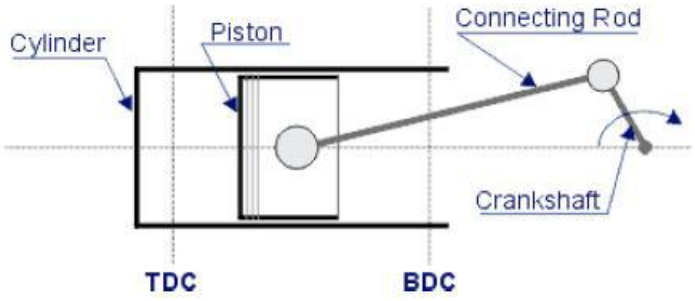

Figure 3.1. Basic Components an Engine (Abdulvahitoglu, 2009)

3.1. Operation of Four-Stroke Engines

In four-stroke engines, the combustion cycle is finished in four strokes. A schematic illustration of a diesel engine's four-stroke combustion cycle may be seen in Figure 3.2. The piston travels from top dead center (TDC) to bottom dead center (BDC) during the first stroke, also referred to as the intake stroke. The cylinder is filled with filtered air throughout the most of this stroke. The air that was previously pulled in during the intake stroke is compressed by the piston as it goes from bottom dead center (BDC) to top dead center (TDC) during the second stroke. The temperature of the air within the cylinder rises throughout this compression stroke, frequently rising beyond the fuel injected close to TDC's auto-ignition temperature. The fuel emits heat energy during ignition and burning, which raises the cylinder pressure considerably as the volume approaches TDC. The piston is forced lower toward BDC by the increased pressure acting on its upper surface.

Exhaust stroke: Combustion byproducts are released into the atmosphere via the exhaust system during the last phase of the four-stroke cycle. In order to maximize specific power output, modern four-stroke diesel engines usually include technology that improve air intake efficiency and enable accurate fuel injection in proportion to the increased air intake. Because the piston moves toward bottom dead center (BDC) during this period of the stroke due to pressure applied to it, it is known as the expansion stroke.

Because of its vital function in harnessing the strength of expanding gasses, it is often referred to as the "power stroke." Furthermore, it is also referred to as the "work stroke," emphasizing how the expanding gases pressurize the piston to do mechanical work (Abdulvahitoglu,2009) .

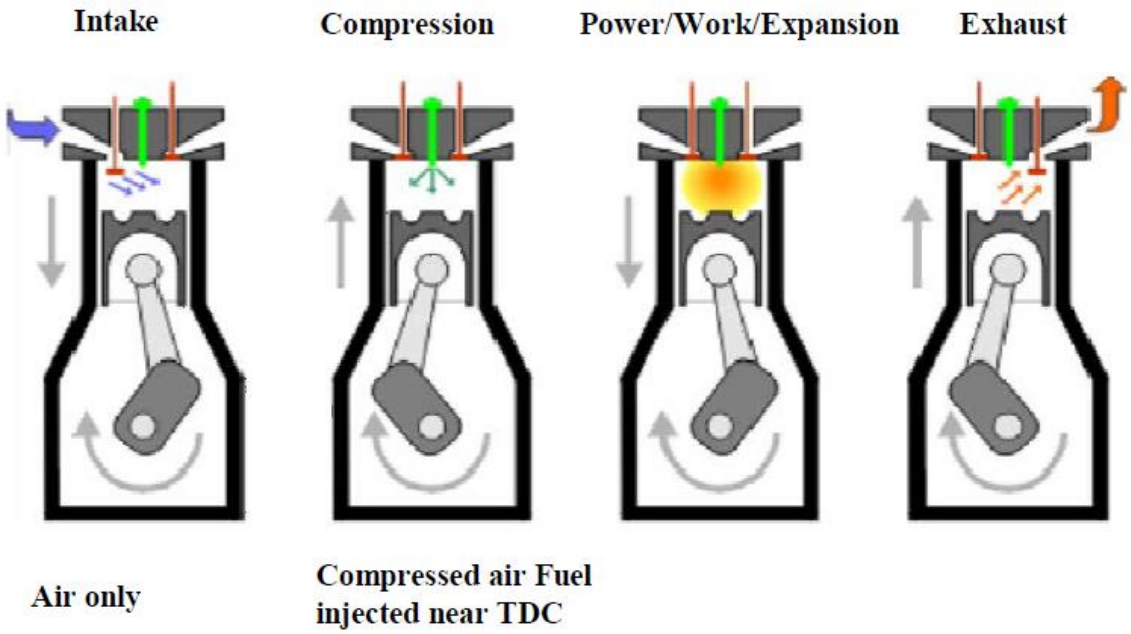

Figure 3.2. 4 stroke diesel operation (Abdulvahitoglu,2009)

During the intake stroke of naturally aspirated engines, the pressure within the cylinder is usually lower than the ambient pressure. A number of components that create constraints, including the air intake filter, air inlet pipe, intake manifold, intake port, and intake valve, have an impact on this pressure drop. After combustion, the piston moves from top dead center (TDC) to bottom dead center (BDC) during the expansion stroke, which is marked by a sequence of chemical reactions and heat transfer processes. Due to the pressure difference between the exhaust system and the cylinder, part of the combustion byproducts are released during the blowdown process, which is started at Cycle No. 3 when the exhaust valve opens. During the exhaust stroke, when the piston travels from BDC to TDC, the residual exhaust gases leave the cylinder (Abdulvahitoglu, 2009).

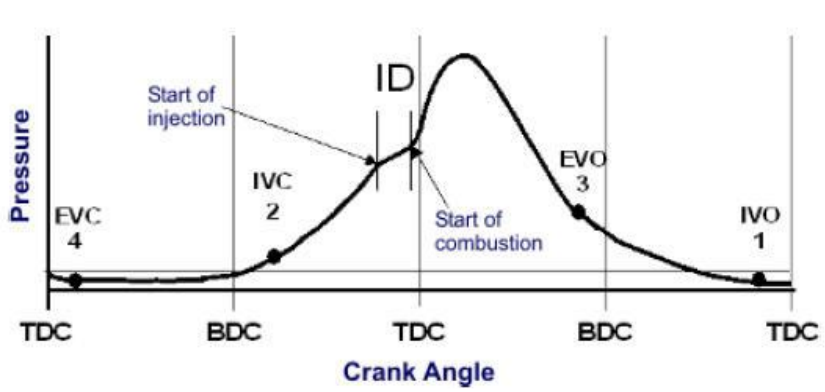

ID – ignition delay;
EVC – exhaust valve closing
IVC – intake valve closing
TDC –top dead center
BDC – bottom dead center
EVO – exhaust valve open
IVO –intake valve open

Figure 3.3. P-CA Diagram for Diesel Engine (Abdulvahitoglu, 2009)

Apart from the information given in the explanation of the pressure-volume diagram, Figure 3.4, the pressure-crank angle diagram, shows important events such fuel injection (I) and ignition delay. Fuel injected into the cylinder uses the heat from the compressed working fluid to evaporate during this delay time.

Cylinder pressure increases rapidly following the start of combustion and peaks a few degrees beyond top dead center (TDC). This sudden spike in pressure is caused by a number of factors, including injection rate, fuel quality, and ignition delay. Many engine designs have a strong correlation between the rate of pressure rise within the cylinder and characteristics like noise, vibration, and harshness. A variety of variables, including fuel quantity, injection time, fuel quality (particularly calorific value and cetane number), starting cylinder pressure at intake valve closing, and charge temperature, all affect the cylinder temperature as it increases and reaches its peak.

In the past, the functioning of intake and exhaust valves was examined using pressure-volume or pressure-crank angle diagrams, and valve overlap was emphasized as a crucial element affecting engine performance and emissions characteristics. An in-depth analysis of the timing and functioning of these valves provides important information on how they affect engine performance, specifically with regard to charge composition and volumetric efficiency.

It opens towards the conclusion of the power stroke, starting with the exhaust valve. Exhaust valve opening (EVO) timing is critical; opening it too soon exposes the system to energy loss, while opening it at the right time guarantees effective exhaust gas clearance during blowdown. To guarantee complete exhaust gas evacuation, the exhaust valve usually stays open for a few degrees after top dead center (TDC). It's important to realize that the intake and exhaust valves

go through a progressive transition from entirely closed to fully open over a predetermined period of time, rather than reaching full openness instantly.

For these valves to operate at their best, they must fully open at the exact moment that they come into contact with the greatest pressure differential. This allows the working fluid to flow smoothly and effectively.Intake and exhaust valves are usually timed to open exactly before their respective strokes, intake and exhaust, to maximize the efficiency of the filling and emptying operations of the cylinder. This method efficiently controls the flow of exhaust gas and intake charge. To improve efficiency, these valves are also left open a few degrees after their strokes are finished.

The piston has less work to do during the exhaust stroke because exhaust gases are released using their own kinetic energy when the exhaust valve opens. In order to prepare for the intake of a new, sufficient charge required for combusting the tiny amount of gasoline injected into the cylinder, this guarantees complete elimination of all exhaust products from the cylinder.

As the exhaust valve opens at the end of the exhaust stroke, the intake valve opens in tandem with the exhaust gasses' high-velocity exit. A pressure differential is created in the cylinder by this quick exhaust flow, which makes it easier to suck in a new charge and maximizes induction efficiency. Opening the intake valve too soon, though, runs the danger of letting some exhaust fumes into the engine through the intake port and enter the intake manifold.

These impurities might re-enter the cylinder on the next intake stroke, jeopardizing the integrity of the new charge.Their timing needs to be closely synchronized with piston position in order to guarantee effective valve action. When interference arises, there are two typical fixes used: valve cutouts in the piston crown or valve recesses in the cylinder head. Smoother valve functioning is made possible by these design elements without sacrificing engine performance.Because of this, it is imperative to carefully plan the opening, closing, lift, flow

The following steps are involved in the combustion process:

Ignition delay (ab): Towards the end of the compression stroke, fuel is delivered straight into the cylinder. The liquid fuel atomizes during injection, forming tiny droplets that enter the combustion chamber. The fuel then turns to vapor and combines with the hot, pressurized air within the chamber.

Premixed combustion phase (bc): During the ignition delay period, a few degrees of crankshaft rotation are all that is needed for the fuel mixed with air to ignite within the flammability restrictions (high temperatures and high pressure).

Mixing-Controlled combustion phase (cd): The pace at which the mixture becomes accessible for combustion is the main factor influencing the rate of burning after the premixed gas has been consumed. The fuel-air mixing process primarily regulates the burning rate during this phase.

Late combustion phase (de): Even without further fuel injection during this phase, heat release may continue at a decreased rate deep into the expansion stroke.

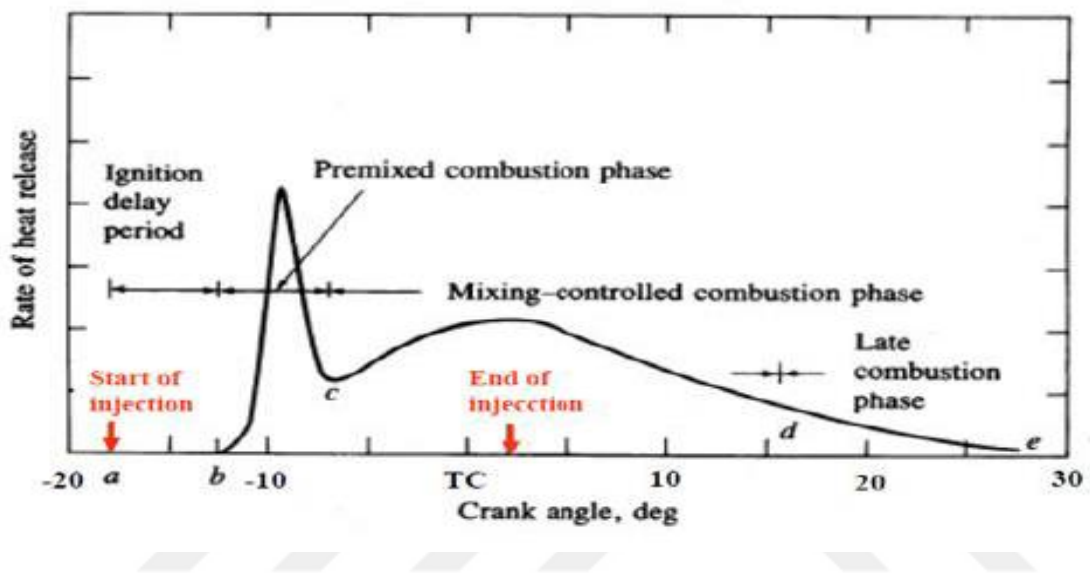

Figure 3.4. Combustion steps in diesel engine (Abdulvahitoglu, 2009)

3.1.1. Ignition Delay

The time or crankshaft angle that passes between the beginning of fuel injection and the start of combustion is referred to as the ignition delay. Before much of the chemical energy of the injected liquid is released during this time, physical and chemical processes must take place.These procedures include the atomization of fuel spray, evaporation, and mixing of fuel vapor with cylinder air on a physical level. High cylinder pressure (with a big divergence angle), tiny injector hole sizes, ideal fuel viscosity, and high fuel injection pressure are necessary to achieve excellent atomization. Fuel volatility, droplet diameter, velocity, and the air pressure and temperature within the cylinder all affect how quickly fuel vaporizes in droplets. Chemical processes resemble those seen in premixed fuel-air mixture autoignition phenomena, but they are more complicated because of the heterogeneous reactions that take place on the liquid fuel droplets' surface (Abdulvahitoglu, 2009).

3.1.1.1. Fuel ignition quality

Fuel's ignition properties, which are mostly determined by its cetane number (CN), have a substantial influence on the fuel's igniting delay. Low cetane number fuels take longer to ignite, requiring the majority of the fuel to be injected before autoignition, which quickens combustion. In extreme circumstances, this quick burning produces a loud banging sound called "diesel knock."On the other hand, fuels with a high cetane number have a shorter ignition delay and require less fuel to ignite automatically. Because the rate of fuel injection and effective fuel-air mixing control the amount of heat escape, this leads to smoother engine running (Abdulvahitoglu, 2009).

One important factor that indicates the weight of a fluid unit volume is its density. There is more energy content per unit volume at higher densities. Performance is improved because the engine gets more energy as the density rises and the amount of fuel injected stays constant. Richer mixes with a greater density, however, might result in higher exhaust emissions, especially particulate matter, when operating at full load.On the other hand, higher volumetric fuel use is generally associated with lesser density (Van Basshuysen and Schäfer, 2004).

Viscosity, which reflects a fluid's thickness and flow properties, specifies the fluid's resistance to deformation or flow. Viscosity in diesel fuel typically increases with density. For the fuel injection system's moving parts to be properly lubricated, viscosity must be maintained above a minimal level.However, high viscosity can compromise proper mixture formation and potentially reduce efficiency while increasing soot emissions due to bigger droplet sizes during high-pressure injection. According to Van Basshuysen and Schäfer (2004), the viscosity of diesel fuel first rises dramatically as temperature rises and then gradually decreases at a slower pace. This temperature-dependent response emphasizes how important viscosity monitoring is for efficiently maximizing engine output and emissions.

The **Higher Heating Value** (HHV) quantifies the total heat released when a fuel undergoes complete combustion and the resulting products return to a reference temperature.

The properties of a fuel's ignition and combustion quality are gauged by its cetane number. Better ignition characteristics are indicated by a higher cetane number, which affects a range of engine performance metrics including noise levels, white smoke emission, stability, drivability, and the emission of CO and HC in addition to combustion efficiency and noise levels.Higher cetane numbers are often associated with smoother performance, easier starting, and less

tendency to knock, especially during cold starts and under variable load circumstances Abdulvahitoglu, Aydin , 2012).

3.7. Emission Types

Five categories of emissions are included by the emissions effect analysis: carbon dioxide (CO2), nitrogen oxides (NOx), particulate matter (PM), hydrocarbons (HC), and carbon monoxide (CO). Although carbon dioxide (CO2) is not a dangerous air toxin, it is regarded as a greenhouse gas emission that contributes to global warming and may occasionally be able to provide emissions credits (Strong et al, 2004).

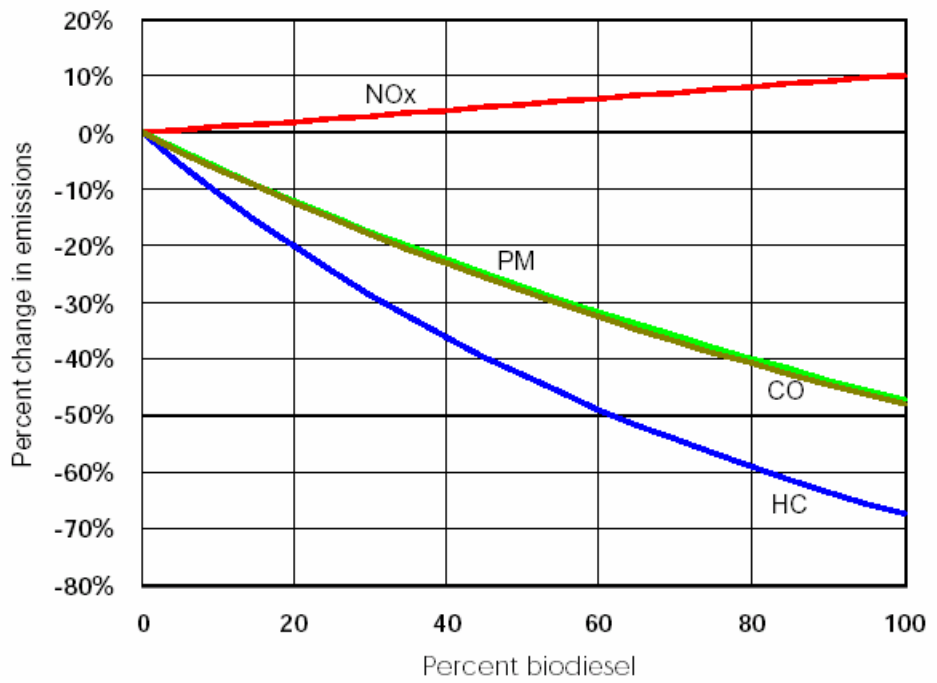

Figure 3.5. Biodiesel effects on pollutant emissions for heavy –duty engines (Strong et al, 2004).

Unburned Hydrocarbon Organic chemicals known as UHC are discharged into the engine exhaust as a result of incomplete fuel combustion. These hydrocarbons can be made up of different molecules, such propane (C_3H_8), ethane (C_2H_6), and methane (CH_4). UHCs contribute significantly to air pollution and have a number of serious consequences. Environmental Impact: UHCs have a negative impact on both the environment and human health by helping to create ground-level ozone and smog. One of the main causes of smog, ground-level ozone, can lead to health concerns, including respiratory ailments.Health Effects:

Breathing difficulties, eye discomfort, and other conditions may arise from exposure to UHCs. Additionally recognized to be carcinogenic are several of the hydrocarbons found in UHCs.

The incomplete combustion of carbon-based fuels, such as charcoal, wood, kerosene, gas, or oil, results in the production of carbon monoxide (CO). CO does not irritate the skin and is tasteless, odorless, or colorless like many other gases. The Centers for Disease Control and Prevention (CDC) state that red blood cells are more attracted to carbon monoxide than to oxygen. Red blood cells may substitute carbon monoxide (CO) for oxygen when there is a substantial concentration of CO in the atmosphere. This might result in tissue damage, carbon monoxide poisoning, or even death.Headaches, weariness, and nausea are among the symptoms that may become more apparent as CO levels rise and surpass 70 parts per million (ppm). Over 150 to 200 parts per million, people run the danger of passing away, becoming disoriented, and losing consciousness (Strong et al, 2004).

Carbon dioxide (CO_2) is one of the harmful gas that linked to global warming. Human activities including burning solid waste, wood and wood products, and fossil fuels (coal, oil, and natural gas) emit it into the atmosphere. The gas carbon dioxide is not hazardous in and of itself. However, it may cause health problems due to its effect on the environment (2004 Strong et al.)

Nitrogen oxides (NO_x) are a class of very reactive gases that include nitrogen and oxygen in different proportions. These gases include nitrogen dioxide (NO_2), nitrates (NO_3–), nitrous oxide (N_2O), and nitric oxide (NO). Ozone may be produced when NO_x and volatile organic compounds react with sunshine and hot, stagnant air. NO_x are categorized as dangerous airborne pollutants because of the harm they do to the environment and human health. According to the U.S. Environmental Protection Agency (EPA), NO_x has a significant role in the development of acid rain, the degradation of water quality, respiratory conditions including bronchitis and emphysema, and ground-level ozone (smog) (Strong et al, 2004).

4.MATERIAL AND METHODS

The integration of MCDM methods in mechanical engineering is essential for addressing the complexity and multifaceted nature of modern engineering problems. These methods provide a systematic and structured approach to decision-making, enabling engineers to evaluate multiple criteria, balance trade-offs, and make informed choices. From material selection and design optimization to supplier selection and project management, MCDM methods enhance the decision-making process across various domains in mechanical engineering. As engineering challenges continue to evolve, the importance of MCDM methods in achieving optimal and sustainable solutions will only grow.

4.1 Research Design

The research design outlines the framework and methodology for investigating the impacts of graphene-doped fuel blends on greenhouse gas emissions using a Multi-Criteria Decision Making (MCDM) approach. This section will detail the steps involved in the research process, including data collection, criteria selection, and the application of MCDM methods.

4.1.1 Research Approach

This study adopts a quantitative research approach to systematically evaluate the effects of graphene-doped fuel blends. The use of MCDM methods allows for the integration of multiple criteria to assess the overall impact on greenhouse gas emissions and related factors.

4.1.2.1 Standard deviation method

The standard deviation method is a technique used for weighting criteria. In probability and statistics, the standard deviation (σ) of a probability distribution is a measure of the dispersion of values (Demir, 2021) In the standard deviation method, it is important to normalize the criteria because of the differences in scale of the data. A prominent feature of this method is that it mitigates the effect of subjectivity from decision-makers and effectively utilizes decision information. The standard deviation method has been used in many decision-making problems in the literature (Demir, 2021)

Step A: Creating a decision matrix

An m×n decision matrix (X) is created, consisting of m rows and n columns, representing the alternatives and criteria respectively.

$$A_{ij} = \begin{bmatrix} a_{11} & a_{12} & \cdots & a_{1n} \\ a_{21} & a_{22} & \cdots & a_{2n} \\ \cdot & \boxdot & \boxdot & \cdot \\ \cdot & \boxdot & \boxdot & \cdot \\ a_{m1} & a_{m2} & \cdots & a_{mn} \end{bmatrix}, \; a_{ij} = \frac{1}{a_{ji}} \quad (1)$$

Step B: matrix normalisation

The decision matrix is normalized using the vector normalization technique, which is calculated with Equation (2).

$$r_{ij} = \frac{x_{ij}}{\sqrt{\sum_{i=1}^{m} x_{ij}^2}} \quad (2)$$

STEP 3: Weighting the Criteria

The standard deviations for each column of the normalized decision matrix elements are calculated using Equation (3).

$$\sigma_j = \sqrt{\frac{\sum_{i=1}^{m} \left(r_{ij} - \bar{r}_{ij}\right)^2}{m}} \quad (3)$$

Subsequently, the weights of the criteria are calculated using Equation (4) based on the standard deviation values.

$$w_j = \frac{\sigma_j}{\sum_{i=1}^{n} \sigma_j} \quad (4)$$

4.1.2.2 Technique for Order Preference by Similarity to Ideal Solution (TOPSIS)

Hwang and Yoon created the TOPSIS method in 1981. It is based on the aggregate Euclidian distance measure between the decision matrix's weighted normalized elements and the best and worst values for each criterion. The ratio of the relative aggregate distance from the worst solutions to the total distances from the best and worst solutions, as well as the selection of the distances from the positive and negative ideal solutions, determines the final ranking. The possibilities are arranged based on specific criteria using the TOPSIS approach (Abdulvahitoğlu et al., 2021; Abdulvahitoglu and Kilic, 2022).

STEP A: Creating a decision matrix.

There must be a decision matrix created. Considering the equation 1, the elements are displayed in columns, while the rows represent the decision points.

STEP B: Matrix normalisation

The squares of each a_{ij} values are calculated, normalized values are determined by using equation 5.

$$r_{ij} = \frac{a_{ij}}{\sqrt{\sum_{k=1}^{m} a_{kj}{}^2}}, i = 1, \dots, m \; j = 1, \dots, n \tag{5}$$

$$R_{ij} = \begin{bmatrix} r_{11} & r_{12} & \cdots & r_{1n} \\ r_{21} & r_{22} & \cdots & r_{2n} \\ \cdot & \square & \square & \cdot \\ \cdot & \square & \square & \cdot \\ r_{m1} & r_{m2} & \cdots & r_{mn} \end{bmatrix} \tag{6}$$

STEP C: Constructing weighted normalized decision matrix

The calculated weight from standart deviation method used for constructing a weighted normalized decision matrix.

$$V_{ij} = \begin{bmatrix} v_{11} & v_{12} & \cdots & v_{1n} \\ v_{21} & v_{22} & \cdots & v_{2n} \\ \cdot & \square & \square & \cdot \\ \cdot & \square & \square & \cdot \\ v_{m1} & v_{m2} & \cdots & v_{mn} \end{bmatrix} = \begin{bmatrix} w_1 r_{11} & w_2 r_{12} & \cdots & w_j r_{1j} & \cdots & w_n r_{1n} \\ w_1 r_{21} & w_2 r_{22} & \cdots & \square & \cdots & r_{2n} \\ \cdot & \square & \square & \square & \square & \cdot \\ w_1 r_{i1} & \square & \square & w_j r_{ij} & \square & w_n r_{in} \\ \cdot & \square & \square & \square & \square & \cdot \\ w_1 r_{m1} & w_2 r_{m2} & \cdots & w_j r_{mj} & \cdots & w_n r_{mn} \end{bmatrix} \tag{7}$$

STEP D: Acquiring the values of the Positive and Negative Ideal Solutions

Eq. (7), which is used to generate the weighted normalised decision matrix, determines the maximal values of each column.

Positive ideal solution values

$$A^+ = \left\{ \max_i \; v_{ij} \,\middle|\, (j \in J), \quad \left(\min_i \; v_{ij} \right) j \in J' \right\} \tag{8}$$

$$A^+ = \{v_1^+, v_2^+, \dots, v_n^+\}$$

$$A^- = \left\{ \min_i \; v_{ij} \,\middle|\, (j \in J), \quad \left(\max_i \; v_{ij} \right) j \in J' \right\} \tag{9}$$

$$A^- = \{v_1^-, v_2^-, \dots, v_n^-\}$$

Where $J = \{j = 1,2, \dots n | j \; associated \; with \; benefit \; criteria\}$,

$J' = \{j = 1,2, \dots n | j \; associated \; with \; cost \; criteria\}$

STEP E: Positive ideal (S^+) and Negative ideal S^- distance values developing

Positive Ideal distance (S^+) developed from equation 8.

$$S_i^+ = \sqrt{\sum_{j=1}^{n}(v_{ij} - v_j^+)^2} \tag{10}$$

Negative ideal distance (S^-) developed from equation 9.

$$S_i^- = \sqrt{\sum_{j=1}^{n}(v_{ij} - v_j^-)^2} \tag{11}$$

STEP F: Finding the relative proximity to the optimal solution (C_i^*) equation 12 calculates the relative proximity to an ideal solving solution based on ideal and non-ideal point spacing.

$$C_i^* = \frac{S_i^-}{S_i^- + S_i^+} \tag{12}$$

4.1.2.3 Complex Proportional Assessment (COPRAS) method

The Complex Proportional Assessment technique was introduced to the literature in 1996 by Zavadskas and Kaklauskas (Demir et al., 2021). It is employed to evaluate and rank solutions while accounting for the criterion's cost and benefit characteristics (Demir, 2021). This method differs from previous MCDM techniques in that it allows alternatives to be compared to one another and their relative superiority to be stated as a percentage. The following is how this method is applied:

STEP A: Creating a decision matrix.

Similarly, equation 1 is used.

STEP B: Matrix normalisation

Normalization for COPRAS is given below, where X^* is normalized decision matrix, elements of which are represented by x_{ij}^*.

$$x_{ij}^{*} = \frac{a_{ij}}{\sum_{i=1}^{m} a_{ij}} \qquad (i = 1, \dots, m \; and \; j = 1, \dots p) \tag{13}$$

STEP C: Constructing weighted normalized decision matrix

The weighting of the normalized decision matrix is determined using equation 14 and the weights (w_i) gained from standart deviation method.

$$n_{ij} = x_{ij}^{*} w_j \tag{14}$$

STEP D: Calculation of S_i^+ and S_i^- values

S_i^+ represents the sum of utility criteria in a weighted normalized decision matrix.

S_i^- represents the sum of cost criteria in a weighted normalized decision matrix

STEP E: Computation of relative significance values.

Equation 14 is employed to obtain relative significance values.

$$Q_i = S_i^+ + \frac{\sum_{i=1}^{m} S_i^-}{S_i^- \sum_{i=1}^{m} \left(\frac{1}{S_i^-}\right)} \tag{15}$$

STEP F: Calculation of the value of the performance index.

Performance index is calculated with equation 16.

$$P_i = \left(\frac{Q_i}{Q_{max}}\right) * 100 \tag{16}$$

4.1.2.4 Multi-Objective Optimization based on Simple Ratio Analysis (MOOSRA)

As a technique for ranking choices, M.C. Das, B. Sarkar, and S. Ray introduced MOOSRA (Multi-Objective Optimization based on Simple Ratio Analysis) to the literature in 2012 (Demir et al., 2021). One technique for multi-objective optimization is the MOOSRA approach. Specifically, creating the problem's decision matrix is the first stage, and normalizing the decision matrix is the second. The MOOSRA technique uses the simple ratio of the sum of the normalized performance values for advantageous criteria to the sum of the normalized

performance values for non-beneficial criteria to determine the overall performance score of each alternative.

$$X^* = \begin{bmatrix} x_{11}^* & \dots & x_{1p}^* \\ \vdots & \ddots & \vdots \\ x_{m1}^* & \dots & x_{mn}^* \end{bmatrix} \qquad (i = 1, \dots, m \; and \; j = 1, \dots n) \tag{17}$$

$$x_{ij}^* = \frac{x_{ij}}{\sum_{i=1}^{m} x_{ij}^2} \tag{18}$$

The elements of the weighted decision matrix are given in equation 19 by using wights calculated from standart deviation method.

$$a_{ij} = x_{ij}^* . w_j \tag{19}$$

Equation 20 is used for the determination of performance scores for the alternatives

$$Y_i = \frac{\sum_{j}^{g} x_{ij}^* . w_j}{\sum_{j'=g+1}^{n} x_{ij'}^* . w_j} \quad , \quad j = 1,2, \dots, g \text{ for beneficial, } j' = g+1, g+2, \dots, n \text{ for cost} \tag{20}$$

Ranking of the alternatives is obtained according to the overall performance score of each alternative. The alternative with the highest overall performance score is the best. By multiplying the criterion weight values w_j obtained by standart deviation method, matrix values are weighted. After normalizing each criterion, the best value is assigned a value of 1, and the worst value is assigned a value of 0. The matrix is then normalized using cost-actuated equation 38, unless the direction of the criteria is advantageous in which case equation 37 is employed.

4.1.2.5 Multi Attributive Ideal Real Comparative Analysis (MAIRCA)

MAIRCA was introduced into the literature by D. Pamucar, L. Vaxin, and V. Lukovac in 2014 for ranking alternatives. It is based on determining the difference between theoretical and actual preference levels. Unlike other MCDM methods, it starts with the assumption that the selection probabilities of all alternatives are equal.

STEP A Creating the decision matrix

$$X^* = \begin{bmatrix} x_{11}^* & \dots & x_{1p}^* \\ \vdots & \ddots & \vdots \\ x_{m1}^* & \dots & x_{mn}^* \end{bmatrix} \qquad (i = 1, \dots, m \; and \; j = 1, \dots n) \qquad (21)$$

STEP B Creating the normalized matrix.

For beneficial criteria eq 22.for cost criteria eq 23 used

Beneficial $n_{ij} = \frac{x_{ij} - x_i^-}{x_i^+ - x_i^-}$ (22)

Cost $n_{ij} = \frac{x_{ij} - x_i^+}{x_i^- - x_i^+}$ (23)

Where $x_i^+ and \; x_i^-$ are maximum and minimum values of th columns.

Normalized matrix formed

$$N = \begin{bmatrix} n_{11} & \dots & n_{1n} \\ \vdots & \ddots & \vdots \\ n_{m1} & \dots & n_{mn} \end{bmatrix} \quad (24)$$

STEP C Determining the selection probabilities of the alternatives

For m alternatives, each has a selection probability of 1/m , and all alternative selection probabilities (Pi) are equal. Equation 25 is used to calculate this probability value.

$P_i = P_{i+1} = \dots = P_m = 1/m$ (25)

STEP D Creating the Theoretical Evaluation Matrix (T)

The elements of the Theoretical Evaluation Matrix are given in equation (26). The weights used in this formula was obtained from standart deviation method.

$t_{ij} = P_i * w_{ij}$ (26)

STEP E Creating the real evaluation matrix (R)

The elements of the Real Evaluation Matrix are given in equation (27).

$r_{ij} = t_{ij} * n_{ij}$ (27)

$$R = \begin{bmatrix} t_{11}n_{11} & \dots & t_{1n}n_{1n} \\ \vdots & \ddots & \vdots \\ t_{11}n_{m1} & \dots & t_{mn}n_{mn} \end{bmatrix} (28)$$

STEP F Creating the total fraction matrix g

The total fraction matrix G is calculated using equation number 29.

$$G = T - R \ (29)$$

$$G = \begin{bmatrix} t_{11} - r_{11} & \dots & t_{1n} - r_{1n} \\ \vdots & \ddots & \vdots \\ t_{m1} - r_{m1} & \dots & t_{mn} - r_{mn} \end{bmatrix} (30)$$

STEP G Calculating Criterion Function Values (Q) for Alternatives

The values of criterion function for each alternative are given in equation number 31.

$Q_i = \sum_j^n g_{ij}$ (31)

4.1.2.6 Multi-Attribute Utility Theory (MAUT)

The Multi-Attribute Utility Theory approach was first published in the literature in 1976 by Keeney and Raiffa (Demir et al., 2021). One of the MCDM strategies for dealing with connection establishment and decision-making challenges is the MAUT strategy. By letting you choose contradicting sections, it provides a research-oriented choice, according to MAUT approaches. Without producing any qualitative or quantitative data, it allows the decision-maker to evaluate every possibility (Ishizaka and Nemery, 2013; Kim and Song, 2009; Zietsman et al., 2006). The following describes the MAUT approach.

$$x_j(a_i) = \frac{x_i(a_i) - min(x)}{\max(x_i) - \min(x_i)} \quad \text{for beneficial} \qquad (32)$$

$$x_j(a_i) = 1 + \frac{x_j - x_i(a_i)}{\max(x_i) - \min(x_i)} \quad \text{for cost} \qquad (33)$$

$$r_{ij} = \frac{e^{(x_{ij})^2} - 1}{1{,}71} \qquad (34)$$

$$x(a_i) = \sum_{j=1}^{q} x_j(a_i).w_j \qquad (35)$$

Where $x(a_i)$ denotes the beneficial value and $x_j(a_i)$ normalized beneficial value, w_j is the weighing values which were calculated by standard deviation method.

4.1.2.7 Multi Objective Optimization on the basis of Ratio Analysis (MOORA) method

The MOORA method was introduced into the literature by Braures and Zavadakas in 2006. This method is very simple and easy to apply, making it highly reliable for addressing various problems in the decision-making process.

Step A Creating the decision matrix

$$X^{\square} = \begin{bmatrix} x_{11}^{\square} & \dots & x_{1p}^{\square} \\ \vdots & \ddots & \vdots \\ x_{m1}^{\square} & \dots & x_{mp}^{\square} \end{bmatrix}$$

Where m is alternative number p is criteria number

Step B Creating the normalized matrix

The elements of the X matrix are used to calculate the normalized decision matrix X^*.Equation 36 is used for the elements x^*_{ij} of the normalized decision matrix.

$$x_{ij}^* = \frac{x_{ij}}{\sum_{i=1}^{m} x_{ij}^2} \qquad (i = 1, \dots, m \; and \; j = 1, \dots p) \; (36)$$

$$X^* = \begin{bmatrix} x_{11}^* & \dots & x_{1p}^* \\ \vdots & \ddots & \vdots \\ x_{m1}^* & \dots & x_{mn}^* \end{bmatrix}$$

Step C Finding the weighted normalized matrix

The elements of the normalized matrix x^*_{ij} are multiplied by the weights w_i to obtain the weighted normalized decision matrix (R) using Equation 37.

$$R = \begin{bmatrix} w_1 x_{11}^* & \dots & w_n x_{1p}^* \\ \vdots & \ddots & \vdots \\ w_1 x_{m1}^* & \dots & w_n x_{mn}^* \end{bmatrix} = \begin{bmatrix} r_{11} & \dots & r_{1p} \\ \vdots & \ddots & \vdots \\ r_{m1} & \dots & r_{mp} \end{bmatrix} \; (37)$$

Step D Obtaining the ranking

The values that determine the ranking are calculated using the elements of the weighted normalized decision matrix with Equation 38.

$$y_j = \sum beneficial\ criteria\ values - \sum cost\ criteria\ values \quad (38)$$

4.1.2.8 Borda method

The Borda technique, developed by Jean-Charles de Borda in 1770, is a voting system used to obtain integrated solutions for multi-criteria decision problems. This method operates using a scoring system based on the rankings of alternatives.

The Borda count (B_i) is calculated as follows:

$$B_i = \sum_{k=1}^{r} m - a_{ik} \quad (39)$$

where m is the number of alternatives.

The points for each alternative are summed up, and this total is the Borda count (Bi) for that alternative. When the Borda counts are calculated, the alternative with the highest total score is considered the best choice.

The decision matrix was constructed utilizing an experimental study contributed to the literature by Hoseini et al. in 2018.

Fuel Blend characteristics

Symbols used in the tables are B denotes for Biodiesel and G denotes for Graphen nanoparticle. Fuel blend symbols and their meanings are shown in Table 1.

Table 1. Fuel blend symbols and their meanings (Hoseini)

Symbol	Meaning	Symbol	Meaning	Symbol	Meaning
B0G0	100% diesel	B10 G0	90% diesel 10% biodiesel	B20 G0	80% diesel 20% biodiesel
B0G30	100% diesel 30 ppm graphen	B10G30	90% diesel 10% Biodiesel 30 ppm graphen	B20G30	80% diesel 20% Biodiesel 30 ppm graphen
B0G60	100% diesel 60 ppm graphen	B10G60	90% diesel 10% Biodiesel 60 ppm graphen	B20G60	80% diesel 20% Biodiesel 60 ppm graphen
B0G90	100% diesel 90 ppm graphen	B10G90	90% diesel 10% Biodiesel 90 ppm graphen	B20G90	80% diesel 20% Biodiesel 90 ppm graphen

Table 2. Fuel properties of blends (Hoseini et al, 2018)

Fuel Blend	Density (g/cm3)	Kinematic viscosity (mm2/s)	Higher Heating Values (Mj/kg)	Cetane Number
B0G0	0.83	5.4645	45.7132	46
B0G30	0.8223	5.4423	45.8312	46.5
B0G60	0.8211	5.4091	45.8268	47
B0G90	0.8206	5.4213	45.9489	47
B10G0	0.8345	5.5338	44.1101	46.5
B10G30	0.8331	5.5103	44.6534	47
B10G60	0.8324	5.4991	44.832	47.5
B10G90	0.8327	5.5011	44.7892	47.5
B20G0	0.8381	5.564	43.6318	47
B20G30	0.837	5.5332	43.9318	47.5
B20G60	0.8364	5.5201	44.0149	48.5
B20G90	0.8369	5.5291	44.0134	48.5

Brake Power is define as the rate of work performed by the engine. Fuel properties such as heating value and viscosity have imortant effects on engine power.

Spesific fuel consumption (SFC) is a measure of the efficiency of an engine. It is typically expressed in terms of the amount of fuel consumed per unit of power produced.

Table 3.Engine operating characteristics of blends (Hoseini et al 2018)

Fuel Blend	Brake Power	SFC
B0G30	4.15084	404.5184
B0G60	4.35379	393.744
B0G90	4.49565	384.8
B10G0	3.97823	424
B10G30	4.191463	384.7
B10G60	4.374064	380.88
B10G90	4.607188	376.89
B20G0	3.9073	438
B20G30	4.242156	398.14
B20G60	4.39454	385.35
B20G90	4.455494	374.58

Table 4. Emissions results (Hoseini et al 2018)

Fuel Blend	CO	CO2	UHC	NOx
B0G0	1.36	3.7	227.79	145.38
B0G30	1.32	3.67	211,98	146.91
B0G60	1.29	3.65	201.12	148.35
B0G90	1.27	3.65	191.94	153.11
B10G0	1.24	3.37	204.37	148.1
B10G30	1.18	3.51	185.11	149.21
B10G60	1.11	3.55	176.34	153.99
B10G90	1.01	3.61	166.7	155.96
B20G0	1.21	3.35	171.13	162.32
B20G30	1.12	3.43	148.34	167.9
B20G60	1.09	3.55	135.83	170.32
B20G90	1.11	3.77	124.12	174.32

The sysmbols attributed to the criterion shown in table 5

Table 5. Criterion

Criteria	Symbol
Density	C1
Kinematic Viscosity	C2
Higher Heating Values	C3
Cetane Number	C4
Brake Power	C5
SFC	C6
CO	C7
CO2	C8
UHC	C9
NOx	C10

The blends were symbolized as alternatives as seen in the table 6

Table 6. Symbols for alternatives of fuel blends

Fuel Blend	Alternative
B0G30	A1
B0G60	A2
B0G90	A3
B10G0	A4
B10G30	A5
B10G60	A6
B10G90	A7
B20G0	A8
B20G30	A9
B20G60	A10
B20G90	A11

Biodiesel blends are shown above at different values. Graphene blends with 0%, 10% and 20% biodiesel fuel at 30, 60, 90 ppm are given. The alternatives of these blends are ranked from A1 to A11. The most suitable of these fuel ratios will be determined at the end with the methods to be applied..

5. RESULTS and DICUSSION

In order to calculate the weight of each criteria standart deviation model was choosen. Using equation 1 the Decision matrix constructed for standard deviation model as seen in table 7.

Table 7. Constructed Decison matrix

	C1	C2	C3	C4	C5	C6	C7	C8	C9	C10
A1	0.8223	5.4423	45.8312	46.5	4.15084	404.5184	1.32	3.67	211.98	146.91
A2	0.8211	5.4091	45.8268	47	4.35379	393.744	1.29	3.65	201.12	148.35
A3	0.8206	5.4213	45.9489	47	4.49565	384.8	1.27	3.65	191.94	153.11
A4	0.8345	5.5338	44.1101	46.5	3.97823	424	1.24	3.37	204.37	148.1
A5	0.8331	5.5103	44.6534	47	4.191463	384.7	1.18	3.51	185.11	149.21
A6	0.8324	5.4991	44.832	47.5	4.374064	380.88	1.11	3.55	176.34	153.99
A7	0.8327	5.5011	44.7892	47.5	4.607188	376.89	1.01	3.61	166.7	155.96
A8	0.8381	5.564	43.6318	47	3.9073	438	1.21	3.35	171.13	162.32
A9	0.837	5.5332	43.9318	47.5	4.242156	398.14	1.12	3.43	148.34	167.9
A10	0.8364	5.5201	44.0149	48.5	4.39454	385.35	1.09	3.55	135.83	170.32
A11	0.8369	5.5291	44.0134	48.5	4.455494	374.58	1.11	3.77	124.12	174.32

After constructing the decisison matrix normalisation was done using equation 2. That is, the square of each of the alternatives was taken and added. Then, the square root of this result was taken and the result was proportioned to each alternative individually. Thus, it was normalized.The normalized matrix shown in table 8.

Table 8.Normalized matrix for standard deviation model

	C1	C2	C3	C4	C5	C6	C7	C8	C9	C10
A1	0.29821	0.29852	0.30916	0.29627	0.29164	0.30837	0.33702	0.31103	0.36233	0.28107
A2	0.29778	0.29670	0.30913	0.29946	0.30590	0.30016	0.32936	0.30934	0.34376	0.28382
A3	0.29760	0.29737	0.30996	0.29946	0.31586	0.29334	0.32426	0.30934	0.32807	0.29293
A4	0.30264	0.30354	0.29755	0.29627	0.27951	0.32322	0.31660	0.28561	0.34932	0.28334
A5	0.30213	0.30225	0.30122	0.29946	0.29449	0.29326	0.30128	0.29747	0.31640	0.28547
A6	0.30187	0.30163	0.30242	0.30264	0.30732	0.29035	0.28340	0.30086	0.30141	0.29461
A7	0.30198	0.30174	0.30214	0.30264	0.32370	0.28731	0.25787	0.30595	0.28493	0.29838
A8	0.30394	0.30519	0.29433	0.29946	0.27453	0.33390	0.30894	0.28391	0.29250	0.31055
A9	0.30354	0.30350	0.29635	0.30264	0.29805	0.30351	0.28596	0.29069	0.25355	0.32123
A10	0.30333	0.30278	0.29691	0.30901	0.30876	0.29376	0.27830	0.30086	0.23217	0.32585
A11	0.30351	0.30328	0.29690	0.30901	0.31304	0.28555	0.28340	0.31950	0.21215	0.33351

Standart deviation calculated using equation 3 and result tabulated in table 9.

Table 9. Standard Deviations

	C1	C2	C3	C4	C5	C6	C7	C8	C9	C10
σ1	0.00233	0.00263	0.00544	0.00414	0.01448	0.01461	0.02368	0.01067	0.04671	0.01792

Weights of each criteria calculated by using equation 4 and results tabulated in table 10.

Table 10. Weights of the criterion

	C1	C2	C3	C4	C5	C6	C7	C8	C9	C10
w	0.01631	0.01847	0.03815	0.02901	0.10154	0.10244	0.16604	0.07484	0.32754	0.12567

The results Show that the most important criteria is the C9 which is UHC (unburned hydro carbon)

Results for TOPSIS method

The constructed decision matrix (Table 11) was normalized by using equation 5 and determined values tabuleted in Table 12.

Table 11. Decision Matrix

	C1	C2	C3	C4	C5	C6	C7	C8	C9	C10
A1	0.0899	0.0900	0.0932	0.0893	0.0880	0.0931	0.1019	0.0938	0.1106	0.0849
A2	0.0898	0.0895	0.0932	0.0903	0.0923	0.0906	0.0996	0.0933	0.1049	0.0857
A3	0.0897	0.0897	0.0935	0.0903	0.0953	0.0885	0.0981	0.0933	0.1001	0.0885
A4	0.0913	0.0915	0.0897	0.0893	0.0844	0.0976	0.0958	0.0862	0.1066	0.0856
A5	0.0911	0.0911	0.0908	0.0903	0.0889	0.0885	0.0911	0.0897	0.0966	0.0862
A6	0.0910	0.0909	0.0912	0.0913	0.0928	0.0876	0.0857	0.0908	0.0920	0.0890
A7	0.0911	0.0910	0.0911	0.0913	0.0977	0.0867	0.0780	0.0923	0.0870	0.0901
A8	0.0916	0.0920	0.0888	0.0903	0.0829	0.1008	0.0934	0.0857	0.0893	0.0938
A9	0.0915	0.0915	0.0894	0.0913	0.0900	0.0916	0.0865	0.0877	0.0774	0.0970
A10	0.0915	0.0913	0.0895	0.0932	0.0932	0.0887	0.0842	0.0908	0.0709	0.0984
A11	0.0915	0.0914	0.0895	0.0932	0.0945	0.0862	0.0857	0.0964	0.0647	0.1007

Determinated value tabulated in table 12.

Table 12. Normalized values R matrix

C1	C2	C3	C4	C5	C6	C7	C8	C9	C10
0.2452	1.6246	14.1694	13.7766	1.2105	124.7420	0.4449	1.1415	76.8057	41.2916
0.2445	1.6049	14.1667	14.0744	1.3318	118.1854	0.4249	1.1291	69.1376	42.1050
0.2442	1.6121	14.2422	14.0744	1.4200	112.8772	0.4118	1.1291	62.9701	44.8503
0.2526	1.6797	13.1252	13.7766	1.1120	137.0464	0.3926	0.9625	71.3901	41.9632
0.2517	1.6655	13.4505	14.0744	1.2343	112.8185	0.3555	1.0441	58.5684	42.5946
0.2513	1.6587	13.5583	14.3755	1.3442	110.5891	0.3146	1.0681	53.1502	45.3674
0.2515	1.6599	13.5324	14.3755	1.4913	108.2842	0.2605	1.1045	47.4979	46.5356
0.2547	1.6981	12.8421	14.0744	1.0727	146.2461	0.3738	0.9511	50.0560	50.4084
0.2541	1.6793	13.0193	14.3755	1.2644	120.8391	0.3203	0.9971	37.6114	53.9337
0.2537	1.6714	13.0686	14.9871	1.3569	113.2001	0.3033	1.0681	31.5352	55.4996
0.2540	1.6769	13.0677	14.9871	1.3948	106.9609	0.3146	1.2045	26.3322	58.1371

In order to calculate weighted nornalized matrix the weights which were calculated (table 10) was used. That is, each criterion of the resulting normalized decision matrix is multiplied by its weight coefficient.Then weighted normalized matrix V was formed (Table 13)

Table. 13 Weighted normalized matrix V

C1	C2	C3	C4	C5	C6	C7	C8	C9	C10
0.003998	0.030005	0.540563	0.399592	0.122916	12.778203	0.073868	0.085432	25.156980	5.189002
0.003987	0.029640	0.540459	0.408232	0.135229	12.106570	0.070548	0.084504	22.645361	5.291225
0.003982	0.029774	0.543343	0.408232	0.144185	11.562808	0.068378	0.084504	20.625273	5.636224
0.004118	0.031023	0.500726	0.399592	0.112905	14.038636	0.065185	0.072036	23.383150	5.273406
0.004104	0.030760	0.513137	0.408232	0.125333	11.556799	0.059030	0.078145	19.183529	5.352750
0.004097	0.030635	0.517250	0.416964	0.136491	11.328425	0.052234	0.079937	17.408863	5.701198
0.004100	0.030657	0.516262	0.416964	0.151428	11.092321	0.043246	0.082662	15.557504	5.848003
0.004153	0.031362	0.489926	0.408232	0.108915	14.981021	0.062069	0.071183	16.395363	6.334687
0.004143	0.031016	0.496686	0.416964	0.128383	12.378409	0.053179	0.074624	12.319279	6.777703
0.004137	0.030869	0.498567	0.434705	0.137772	11.595886	0.050369	0.079937	10.329044	6.974489
0.004142	0.030970	0.498533	0.434705	0.141621	10.956766	0.052234	0.090151	8.624864	7.305931

After creating the weighted decision matrix here, the maximum or minimum values are found depending on the situation in order to reach the ideal solution, whether positive or negative.

Table 14. Solution values

	C1	C2	C3	C4	C5	C6	C7	C8	C9	C10
A^*	0.00415	0.03136	0.54334	0.43471	0.15143	14.03864	0.07387	0.09015	25.15698	7.3059
A^-	0.00398	0.02964	0.48993	0.39959	0.10892	10.95677	0.04325	0.07204	8.62486	5.1890

Table 15. Positive ideal distance

	C1	C2	C3	C4	C5	C6	C7	C8	C9
A1	0.000000024064	0.00000184132	0.00000772855	0.00123	0.00081	1.58869	0.00000	0.00002	0.00000
A2	0.000000027818	0.00000296502	0.00000831639	0.00070	0.00026	3.73288	0.00001	0.00003	6.30823
A3	0.000000029461	0.00000252196	0	0.00070	0.00005	6.12972	0.00003	0.00003	20.53637
A4	0.000000001267	0.00000011528	0.001816231	0.00123	0.00148	0.00000	0.00008	0.00033	31.14647
A5	0.000000002441	0.00000036295	0.000912433	0.00070	0.00068	6.15951	0.00022	0.00014	35.68212
A6	0.000000003170	0.00000052906	0.000680872	0.00031	0.00022	7.34524	0.00047	0.00010	60.03332
A7	0.000000002846	0.00000049714	0.000733362	0.00031	0.00000	8.68077	0.00094	0.00006	92.14994
A8	0	0	0.002853424	0.00070	0.00181	0.88809	0.00014	0.00036	76.76594
A9	0.000000000118	0.00000011989	0.002176886	0.00031	0.00053	2.75635	0.00043	0.00024	164.80658
A10	0.000000000283	0.00000024299	0.002004917	0.00000	0.00019	5.96703	0.00055	0.00010	219.86769
A11	0.000000000141	0.00000015382	0.002007961	0.00000	0.00010	9.49793	0.00047	0.00000	273.31086

Table 16. Negative ideal distance

	C1	C2	C3	C4	C5	C6	C7	C8	C9	C10
A1	0.000000000272	0.00000013320	0.002564149	0	0.00020	3.31763	0.00094	0.00018	273.31086	0.00000
A2	0.000000000023	0	0.002553648	0.000074642	0.00069	1.32205	0.00075	0.00016	196.57434	0.01045
A3	0	0.00000001791	0.002853424	0.000074642	0.00124	0.36729	0.00063	0.00016	144.00982	0.20001
A4	0.000000018506	0.00000191102	0.000116644	0	0.00002	9.49793	0.00048	0.00000	217.80701	0.00712
A5	0.000000014940	0.00000125321	0.000538748	0.000074642	0.00027	0.36004	0.00025	0.00004	111.48539	0.02681
A6	0.000000013302	0.00000098914	0.000746597	0.000301772	0.00076	0.13813	0.00008	0.00006	77.15863	0.26235
A7	0.000000013993	0.00000103397	0.000693626	0.000301772	0.00181	0.01838	0.00000	0.00011	48.06150	0.43428
A8	0.000000029461	0.00000296502	0	0.000074642	0.00000	16.19463	0.00035	0.00000	60.38065	1.31260
A9	0.000000025839	0.00000189246	0.000045702	0.000301772	0.00038	2.02107	0.00010	0.00001	13.64870	2.52397
A10	0.000000023966	0.00000151039	0.000074669	0.001232906	0.00083	0.40847	0.00005	0.00006	2.90423	3.18797
A11	0.000000025522	0.00000176816	0.000074083	0.001232906	0.00107	0.00000	0.00008	0.00033	0.00000	4.48139

According to the results obtained with the TOPSIS method, the positive-negative ideal distance and optimal solution is shown in Table 17.

Table 17. Results for positive- negative ideal distances and optimal solution

Positive ideal Distance		Negative ideal distance		Optimal Solution	
$S1^+$	2.464174948	$S1^-$	16.63227	C1*	0.870961579126
$S2^+$	3.755152214	$S2^-$	14.06809	C2*	0.789311454922
$S3^+$	5.427230283	$S3^-$	12.02423	C3*	0.689009937292
$S4^+$	2.69862274	$S4^-$	15.07689	C4*	0.848183145452
$S5^+$	6.757159907	$S5^-$	10.57702	C5*	0.610182959927
$S6^+$	8.363941766	$S6^-$	8.80688	C6*	0.512897872608
$S7^+$	10.14683713	$S7^-$	6.96542	C7*	0.407042732355
$S8^+$	8.865844685	$S8^-$	8.82544	C8*	0.498857933321
$S9^+$	12.95552578	$S9^-$	4.26551	C9*	0.247691818277
$S10^+$	15.03154736	$S10^-$	2.55008	C10*	0.145042470128
$S11^+$	16.81699599	$S11^-$	2.11759	C11*	0.111837003835

After finding the distances to the positive and negative ideal solutions, the necessary calculations are made and then the results are listed.

Table 18. Final Ranking

Alternative	Symbol	C*	Rank
A1	B0G30	0.870962	11
A2	B0G60	0.789311	9
A3	B0G90	0.689010	8
A4	B10G0	0.848183	10
A5	B10G30	0.610183	7
A6	B10G60	0.512898	6
A7	B10G90	0.407043	4
A8	B20G0	0.498858	5
A9	B20G30	0.247692	3
A10	B20G60	0.145042	2
A11	B20G90	0.111837	1

According to the results obtained: It can be seen from the table 18 that the best value can be obtained from the B20G90 fuel mixture. That is, good results are obtained from the mixture of 20% Biodiesel and 90 ppm graphene oxide.

COPRAS Method

In order to calculate the weight of each criteria standart deviation model was choosen. Using equation 1 the Decision matrix constructed for standard deviation model as seen in table 19.

Table19. Decison matrix for COPRAS method

	C1	C2	C3	C4	C5	C6	C7	C8	C9	C10
A1	0.0899	0.0900	0.0932	0.0893	0.0880	0.0931	0.1019	0.0938	0.1106	0.0849
A2	0.0898	0.0895	0.0932	0.0903	0.0923	0.0906	0.0996	0.0933	0.1049	0.0857
A3	0.0897	0.0897	0.0935	0.0903	0.0953	0.0885	0.0981	0.0933	0.1001	0.0885
A4	0.0913	0.0915	0.0897	0.0893	0.0844	0.0976	0.0958	0.0862	0.1066	0.0856
A5	0.0911	0.0911	0.0908	0.0903	0.0889	0.0885	0.0911	0.0897	0.0966	0.0862
A6	0.0910	0.0909	0.0912	0.0913	0.0928	0.0876	0.0857	0.0908	0.0920	0.0890
A7	0.0911	0.0910	0.0911	0.0913	0.0977	0.0867	0.0780	0.0923	0.0870	0.0901
A8	0.0916	0.0920	0.0888	0.0903	0.0829	0.1008	0.0934	0.0857	0.0893	0.0938
A9	0.0915	0.0915	0.0894	0.0913	0.0900	0.0916	0.0865	0.0877	0.0774	0.0970
A10	0.0915	0.0913	0.0895	0.0932	0.0932	0.0887	0.0842	0.0908	0.0709	0.0984
A11	0.0915	0.0914	0.0895	0.0932	0.0945	0.0862	0.0857	0.0964	0.0647	0.1007

In order to calculate the weighted normalized matrixi is ude by equation 14. Result is shown in table 20.

Table 20. Weighted Normalized Matrix for COPRAS Method

C1	C2	C3	C4	C5	C6	C7	C8	C9	C10
0.0014661	0.0016624	0.0035568	0.0025912	0.0089387	0.0095355	0.0169249	0.0070231	0.0362195	0.0106685
0.0014639	0.0016522	0.0035564	0.0026191	0.0093757	0.0092815	0.0165403	0.0069848	0.0343639	0.0107731
0.0014630	0.0016559	0.0035659	0.0026191	0.0096812	0.0090707	0.0162838	0.0069848	0.0327954	0.0111187
0.0014878	0.0016903	0.0034232	0.0025912	0.0085670	0.0099947	0.0158992	0.0064490	0.0349192	0.0107549
0.0014853	0.0016831	0.0034653	0.0026191	0.0090262	0.0090683	0.0151298	0.0067169	0.0316284	0.0108355
0.0014841	0.0016797	0.0034792	0.0026469	0.0094194	0.0089783	0.0142323	0.0067935	0.0301299	0.0111826
0.0014846	0.0016803	0.0034759	0.0026469	0.0099214	0.0088842	0.0129501	0.0069083	0.0284828	0.0113257
0.0014942	0.0016995	0.0033861	0.0026191	0.0084142	0.0103247	0.0155145	0.0064107	0.0292397	0.0117875
0.0014923	0.0016901	0.0034093	0.0026469	0.0091353	0.0093851	0.0143605	0.0065638	0.0253457	0.0121928
0.0014912	0.0016861	0.0034158	0.0027026	0.0094635	0.0090836	0.0139759	0.0067935	0.0232083	0.0123685
0.0014921	0.0016889	0.0034157	0.0027026	0.0095947	0.0088298	0.0142323	0.0072145	0.0212074	0.0126590
0.0163051	0.0184691	0.0381500	0.0290052	0.1015379	0.1024370	0.1660441	0.0748433	0.3275406	0.1256673

Another process is to take the total of the benefits and losses according to the positive and negative solutions. And each of the benefits and losses is proportioned to each other. And the relative importance values are found using equation 15. At the same time, the maximum value is found among these relative importance values.

Table 21. Results of calculations

	Si+	Si-	1/Si-	Q	Qmax
A1	0.0221	0.0765	13.0758	0.0835883	0.101146014
A2	0.0225	0.0741	13.4998	0.0860080	
A3	0.0229	0.0724	13.8145	0.0878024	
A4	0.0210	0.0747	13.3786	0.0839323	
A5	0.0218	0.0698	14.3203	0.0891573	
A6	0.0223	0.0677	14.7738	0.0918011	
A7	0.0230	0.0648	15.4302	0.0955005	
A8	0.0208	0.0701	14.2734	0.0879391	
A9	0.0218	0.0645	15.5118	0.0946874	
A10	0.0224	0.0618	16.1776	0.0984375	
A11	0.0229	0.0601	16.6362	0.1011460	

According to result of calculations by COPRAS method, the best value of positive negative is shown in table 21.

Then, each of the relative importance values found is divided by the maximum value. And the performance index is found. As shown in Equation 16.

Table 22. Performance indexes

Performans indeks	
P1	82.6412
P2	85.0335
P3	86.8076
P4	82.9814
P5	88.1471
P6	90.7610
P7	94.4185
P8	86.9427
P9	93.6145
P10	97.3222
P11	100.0000

According to the results obtained, it can be seen in the table that the highest performance is P11 which is A11. According to the results obtained: It can be seen from the table 22 that the best value can be obtained from the B20G90 fuel mixture. That is, good results are obtained from the mixture of 20% Biodiesel and 90 ppm graphene oxide.

After the alternative values are found, they are ranked one by one and the best alternative is determined.

Table 23. Ranks according to COPRAS method

Alternatif	Pindeks	Rank
A1	82.64	11
A2	85.03	9
A3	86.81	8
A4	82.98	10
A5	88.15	6
A6	90.76	5
A7	94.42	3
A8	86.94	7
A9	93.61	4
A10	97.32	2
A11	100.00	1

MOOSRA Method

Equation 19 was used to obtain the weight decision matrix. Using this, the decision matrix was normalized.The decision matrix obtained using the MOOSRA method is given in table 24.

Table 24. Decision matrix for MOOSRA Method

	C1	C2	C3	C4	C5	C6	C7	C8	C9	C10
A1	0.0899	0.0900	0.0932	0.0893	0.0880	0.0931	0.1019	0.0938	0.1106	0.0849
A2	0.0898	0.0895	0.0932	0.0903	0.0923	0.0906	0.0996	0.0933	0.1049	0.0857
A3	0.0897	0.0897	0.0935	0.0903	0.0953	0.0885	0.0981	0.0933	0.1001	0.0885
A4	0.0913	0.0915	0.0897	0.0893	0.0844	0.0976	0.0958	0.0862	0.1066	0.0856
A5	0.0911	0.0911	0.0908	0.0903	0.0889	0.0885	0.0911	0.0897	0.0966	0.0862
A6	0.0910	0.0909	0.0912	0.0913	0.0928	0.0876	0.0857	0.0908	0.0920	0.0890
A7	0.0911	0.0910	0.0911	0.0913	0.0977	0.0867	0.0780	0.0923	0.0870	0.0901
A8	0.0916	0.0920	0.0888	0.0903	0.0829	0.1008	0.0934	0.0857	0.0893	0.0938
A9	0.0915	0.0915	0.0894	0.0913	0.0900	0.0916	0.0865	0.0877	0.0774	0.0970
A10	0.0915	0.0913	0.0895	0.0932	0.0932	0.0887	0.0842	0.0908	0.0709	0.0984
A11	0.0915	0.0914	0.0895	0.0932	0.0945	0.0862	0.0857	0.0964	0.0647	0.1007

Normalization was done using Equation 18.The normalized matrix obtained using the MOOSRA method is given in table 25.

Table 25 Normalized Matrix for MOOSRA Method

	C1	C2	C3	C4	C5	C6	C7	C8	C9	C10
A1	0.000859	0.005684	0.047867	0.048566	0.004335	0.422490	0.001379	0.003833	0.221398	0.153437
A2	0.000858	0.005649	0.047863	0.049088	0.004547	0.411237	0.001347	0.003812	0.210055	0.154941
A3	0.000857	0.005662	0.047990	0.049088	0.004695	0.401896	0.001326	0.003812	0.200468	0.159912
A4	0.000872	0.005780	0.046070	0.048566	0.004155	0.442838	0.001295	0.003520	0.213450	0.154680
A5	0.000870	0.005755	0.046637	0.049088	0.004378	0.401792	0.001232	0.003666	0.193334	0.155839
A6	0.000869	0.005743	0.046824	0.049610	0.004568	0.397802	0.001159	0.003708	0.184174	0.160832
A7	0.000870	0.005746	0.046779	0.049610	0.004812	0.393635	0.001055	0.003770	0.174106	0.162889
A8	0.000875	0.005811	0.045570	0.049088	0.004081	0.457460	0.001264	0.003499	0.178733	0.169532
A9	0.000874	0.005779	0.045884	0.049610	0.004431	0.415829	0.001170	0.003582	0.154930	0.175360
A10	0.000874	0.005765	0.045970	0.050655	0.004590	0.402470	0.001138	0.003708	0.141865	0.177887
A11	0.000874	0.005775	0.045969	0.050655	0.004653	0.391222	0.001159	0.003937	0.129634	0.182065

The weighted decision matrix is created by multiplying the normalized decision matrix with the weight coefficient.

Table 26. Weighted Normalized Matrix for MOOSRA method

	C1	C2	C3	C4	C5	C6	C7	C8	C9	C10
A1	0.00001400	0.000105	0.001826	0.001409	0.000440	0.043279	0.000229	0.000287	0.072517	0.019282
A2	0.00001398	0.000104	0.001826	0.001424	0.000462	0.042126	0.000224	0.000285	0.068802	0.019471
A3	0.00001397	0.000105	0.001831	0.001424	0.000477	0.041169	0.000220	0.000285	0.065661	0.020096
A4	0.00001421	0.000107	0.001758	0.001409	0.000422	0.045363	0.000215	0.000263	0.069913	0.019438
A5	0.00001419	0.000106	0.001779	0.001424	0.000445	0.041158	0.000205	0.000274	0.063325	0.019584
A6	0.00001418	0.000106	0.001786	0.001439	0.000464	0.040750	0.000192	0.000277	0.060325	0.020211
A7	0.00001418	0.000106	0.001785	0.001439	0.000489	0.040323	0.000175	0.000282	0.057027	0.020470
A8	0.00001427	0.000107	0.001739	0.001424	0.000414	0.046861	0.000210	0.000262	0.058542	0021305
A9	0.00001425	0.000107	0.001750	0.001439	0.000450	0.042596	0.000194	0.000268	0.050746	0.022037
A10	0.00001424	0.000106	0.001754	0.001469	0.000466	0.041228	0.000189	0.000277	0.046466	0.022355
A11	0.00001425	0.000107	0.001754	0.001469	0.000473	0.040076	0.000192	0.000295	0.042461	0.022880

Among the alternatives, the beneficial and costly ones are collected and ranked.

Table 27. Results of Beneficial and Cost values of alternatives

	Beneficial	Cost
A1	0.06440956362468	0.07497774118962
A2	0.06348250043789	0.07125501193604
A3	0.06316539466206	0.06811622412371
A4	0.06663174770944	0.07227048672066
A5	0.06261056008013	0.06570348966674
A6	0.06286375428957	0.06270121201655
A7	0.06272015751667	0.05938912438541
A8	0.07000358960533	0.06087414425081
A9	0.06652207640894	0.05307983710181
A10	0.06551777781176	0.04880748280961
A11	0.06489698120514	0.04482236475622

According to the Results of Beneficial and Cost values of alternatives; A11 is the best alternative.

Table 28. Ranking of the alternatives according to MOOSRA Method

Alternative	Result	Rank
A1	0.85905	11
A2	0.89092	10
A3	0.92732	8
A4	0.92198	9
A5	0.95293	7
A6	1.00259	6
A7	1.05609	5
A8	1.14997	4
A9	1.25325	3
A10	1.34237	2
A11	1.44787	1

According to the results obtained: It can be seen from the table 28 that the best value can be obtained from the B20G90 fuel mixture. That is, good results are obtained from the mixture of 20% Biodiesel and 90 ppm graphene oxide

MAIRCA Method

The decision matrix was obtained using equation 21 according to the MAIRCA method. It is shown in Table 29.

Table 29. Decision matrix for MAIRCA method

	C1	C2	C3	C4	C5	C6	C7	C8	C9	C10
A1	0.0899	0.0900	0.0932	0.0893	0.0880	0.0931	0.1019	0.0938	0.1106	0.0849
A2	0.0898	0.0895	0.0932	0.0903	0.0923	0.0906	0.0996	0.0933	0.1049	0.0857
A3	0.0897	0.0897	0.0935	0.0903	0.0953	0.0885	0.0981	0.0933	0.1001	0.0885
A4	0.0913	0.0915	0.0897	0.0893	0.0844	0.0976	0.0958	0.0862	0.1066	0.0856
A5	0.0911	0.0911	0.0908	0.0903	0.0889	0.0885	0.0911	0.0897	0.0966	0.0862
A6	0.0910	0.0909	0.0912	0.0913	0.0928	0.0876	0.0857	0.0908	0.0920	0.0890
A7	0.0911	0.0910	0.0911	0.0913	0.0977	0.0867	0.0780	0.0923	0.0870	0.0901
A8	0.0916	0.0920	0.0888	0.0903	0.0829	0.1008	0.0934	0.0857	0.0893	0.0938
A9	0.0915	0.0915	0.0894	0.0913	0.0900	0.0916	0.0865	0.0877	0.0774	0.0970
A10	0.0915	0.0913	0.0895	0.0932	0.0932	0.0887	0.0842	0.0908	0.0709	0.0984
A11	0.0915	0.0914	0.0895	0.0932	0.0945	0.0862	0.0857	0.0964	0.0647	0.1007

The normalized matrix was obtained using equations 22 and 23 according to the MAIRCA method. It is shown in Table 30.

Table 30. Normalized matrix for MAIRCA method

	C1	C2	C3	C4	C5	C6	C7	C8	C9	C10
A1	0.92941	0.72333	0.05080	1.00000	0.34797	0.52793	0.00000	0.25000	0.00000	1.00000
A2	1.00000	1.00000	0.05270	0.75000	0.63794	0.69782	0.09677	0.30000	0.12361	0.94746
A3	1.02941	0.89833	0.00000	0.75000	0.84063	0.83885	0.16129	0.30000	0.22809	0.77381
A4	0.21176	-0.03917	0.79358	1.00000	0.10134	0.22075	0.25806	1.00000	0.08662	0.95659
A5	0.29412	0.15667	0.55910	0.75000	0.40601	0.84043	0.45161	0.65000	0.30583	0.91609
A6	0.33529	0.25000	0.48202	0.50000	0.66691	0.90066	0.67742	0.55000	0.40565	0.74170
A7	0.31765	0.23333	0.50050	0.50000	1.00000	0.96358	1.00000	0.40000	0.51537	0.66983
A8	0.00000	-0.29083	1.00000	0.75000	0.00000	0.00000	0.35484	1.05000	0.46494	0.43780
A9	0.00000	-0.03417	0.87053	0.50000	0.47844	0.62851	0.64516	0.85000	0.72433	0.23422
A10	0.06471	0.07500	0.83466	0.00000	0.69617	0.83018	0.74194	0.55000	0.86672	0.14593
A11	0.10000	0.00000	0.83531	0.00000	0.78326	1.00000	0.67742	0.00000	1.00000	0.00000

The probability values of each alternative are equal. When creating the theoretical evaluation matrix, the probability of each alternative is obtained by multiplying it with the weight coefficient. Equation 26 is also given.

Table 31. T matrix

	Matrix value
$t_{11}=t_{21}=t_{31}=t_{41}=t_{51}=t_{61}=t_{71}=t_{81}=t_{91}=t_{101}$	0.001630511
$t_{12}=t_{22}=t_{32}=t_{41}=t_{52}=t_{62}=t_{72}=t_{82}=t_{92}=t_{102}$	0.001846911
t13=t23=t33=t43=t53= t63=t73=t83=t93=t103	0.003815009
t14=t24=t33=t44=t54= t64=t74=t84=t94=t104	0.002900525
t15=t25=t35=t45=t55= t65=t75=t85=t95=t105	0.01015379
t16=t26=t36=t46=t56= t66=t76=t86=t96=t106	0.010243708
t17=t27=t37=t47=t57= t67=t77=t87=t97=t107	0.016604412
t18= t28=t38=t48=t58= t68=t78=t88=t98=t108	0.007484334
t19= t29=t39=t49=t59= t69=t79=t89=t99=t109	0.032754066
$t_{110}=t_{210}=t_{310}=t_{410}=t_{510}=t_{610}=t_{710}=t_{810}=t_{910}=t_{1010}$	0.012566733

Where $x(a_i)$ denotes the beneficial value and $x_j(a_i)$ normalized beneficial value, w_j is the weighing values which were calculated by standard deviation method by using equation 35.It is shown in table 32.

Table 32. Weighted Normalized matrix for MAIRCA Method

C1	C2	C3	C4	C5	C6	C7	C8	C9	C10
0.92941	0.72333	0.05080	1.00000	0.34797	0.52793	0.00000	0.25000	0.00000	1.00000
1.00000	1.00000	0.05270	0.75000	0.63794	0.69782	0.09677	0.30000	0.12361	0.94746
1.02941	0.89833	0.00000	0.75000	0.84063	0.83885	0.16129	0.30000	0.22809	0.77381
0.21176	-0.03917	0.79358	1.00000	0.10134	0.22075	0.25806	1.00000	0.08662	0.95659
0.29412	0.15667	0.55910	0.75000	0.40601	0.84043	0.45161	0.65000	0.30583	0.91609
0.33529	0.25000	0.48202	0.50000	0.66691	0.90066	0.67742	0.55000	0.40565	0.74170
0.31765	0.23333	0.50050	0.50000	1.00000	0.96358	1.00000	0.40000	0.51537	0.66983
0.00000	-0.29083	1.00000	0.75000	0.00000	0.00000	0.35484	1.05000	0.46494	0.43780
0.00000	-0.03417	0.87053	0.50000	0.47844	0.62851	0.64516	0.85000	0.72433	023422
0.06471	0.07500	0.83466	0.00000	0.69617	0.83018	0.74194	0.55000	0.86672	0.14593
0.10000	0.00000	0.83531	0.00000	0.78326	1.00000	0.67742	0.00000	1.00000	0.00000

The Real Evaluation Matrix according to the MAIRCA method is shown in table 33.

The actual value matrix is obtained by multiplying the normalized decision matrix with the theoretical evaluation matrix. It is shown in Equation 27.

Table 33. Real Evaluation Matrix

C1	C2	C3	C4	C5	C6	C7	C8	C9	C10
0.00151542	0.00133593	0.00019379	0.00290052	0.00353321	0.00540801	0.00000000	0.00187108	0.00000000	0.01256673
0.00163051	0.00184691	0.00020103	0.00217539	0.00647756	0.00714831	0.00160688	0.00224530	0.00404859	0.01190653
0.00167847	0.00165914	0.00000000	0.00217539	0.00853563	0.00859296	0.00267813	0.00224530	0.00747088	0.00972420
0.00034528	-0.0000723	0.00302751	0.00290052	0.00102903	0.00226130	0.00428501	0.00748433	0.00283700	0.01202115
0.00047956	0.00028935	0.00213299	0.00217539	0.00412256	0.00860911	0.00749877	0.00486482	0.01001709	0.01151225
0.00054670	0.00046173	0.00183893	0.00145026	0.00677169	0.00922612	0.01124815	0.00411638	0.01328653	0.00932075
0.00051.793	0.00043095	0.00190940	0.00145026	0.01015379	0.00987059	0.01660441	0.00299373	0.01688031	0.00841756
0.00000000	-0.00053714	0.00381501	0.00217539	0.00000000	0.00000000	0.00589189	0.00785855	0.01522881	0.00550167
0.00000000	-0.00006310	0.00332107	0.00145026	0.00485800	0.00643826	0.01071252	0.00636168	0.02372489	0.00294339
0.00010550	0.00013852	0.00318425	0.00000000	0.00706875	0.00850412	0.01231940	0.00411638	0.02838860	0.00183389
0.00016305	0.00000000	0.00318672	0.00000000	0.00795305	0.01024371	0.01124815	0.00000000	0.03275407	0.00000000

The difference between the reel evaluation matrix and the theoretical evaluation matrix gives the total. It is shown in Equation 29.

Table 34. Total Difference Matrix G

C1	C2	C3	C4	C5	C6	C7	C8	C9	C10
0.000115	0.000511	0.003621	0.000000	0.006621	0.0048357	0.0166044	0.0056133	0.0327541	0.0000000
0.000000	0.000000	0.003614	0.000725	0.003676	0.0030954	0.0149975	0.0052390	0.0287055	0.0006602
-0.000048	0.000188	0.003815	0.000725	0.001618	0.0016508	0.0139263	0.0052390	0.0252832	0.0028425
0.001285	0.001919	0.000788	0.000000	0.009125	0.0079824	0.0123194	0.0000000	0.0299171	0.0005456
0.001151	0.001558	0.001682	0.000725	0.006031	0.0016346	0.0091056	0.0026195	0.0227370	0.0010545
0.001084	0.001385	0.001976	0.001450	0.003382	0.0010176	0.0053563	0.0033680	0.0194675	0.0032460
0.001113	0.001416	0.001906	0.001450	0.000000	0.0003731	0.0000000	0.0044906	0.0158738	0.0041492
0.001631	0.002384	0.000000	0.000725	0.010154	0.0102437	0.0107125	-0.0003742	0.0175253	0.0070651
0.001631	0.001910	0.000494	0.001450	0.005296	0.0038055	0.0058919	0.0011227	0.0090292	0.0096233
0.001525	0.001708	0.000631	0.002901	0.003085	0.0017396	0.0042850	0.0033680	0.0043655	0.0107328
0.001467	0.001847	0.000628	0.002901	0.002201	0.0000000	0.0053563	0.0074843	0.0000000	0.0125667

The criterion function is obtained by summing each of the total values. It is shown in Equation 31.

$$Qi=\sum_{j=1}^{n} g_{ij} \quad \textbf{(31)}$$

Table 35. Criteria Function

Criteria Function Q	Result	Rank
Q1	0.0706753	11
Q2	0.0607130	9
Q3	0.0552399	7
Q4	0.0638812	10
Q5	0.0482981	6
Q6	0.0417328	5
Q7	0.0307711	1
Q8	0.0600658	8
Q9	0.0402530	4
Q10	0.0343406	3
Q11	0.0344513	2

According to table 35; Q7 is the best criteria function. According to the results obtained: It can be seen from the table 37 that the best value can be obtained from the B10G90 fuel mixture. That is, good results are obtained from the mixture of 10% Biodiesel and 90 ppm graphene oxide

MAUT METHOD

Table 36. Decision matrix for MAUT method

	C1	C2	C3	C4	C5	C6	C7	C8	C9	C10
A1	0.8223	5.4423	45.8312	46.5	4.15084	404.5184	1.32	3.67	211.98	146.91
A2	0.8211	5.4091	45.8268	47	4.35379	393.744	1.29	3.65	201.12	148.35
A3	0.82060	5.4213	45.9489	47	4.49565	384.8	1.27	3.65	191.94	153.11
A4	0.83450	5.5338	44.1101	46.5	3.97823	424	1.24	3.37	204.37	148.1
A5	0.83310	5.5103	44.6534	47	4.191463	384.7	1.18	3.51	185.11	149.21
A6	0.83240	5.4991	44.832	47.5	4.374064	380.88	1.11	3.55	176.34	153.99
A7	0.83270	5.5011	44.7892	47.5	4.607188	376.89	1.01	3.61	166.7	155.96
A8	0.83810	5.564	43.6318	47	3.9073	438	1.21	3.35	171.13	162.32
A9	0.83700	5.5332	43.9318	47.5	4.242156	398.14	1.12	3.43	148.34	167.9
A10	0.83640	5.5201	44.0149	48.5	4.39454	385.35	1.09	3.55	135.83	170.32
A11	0.83690	5.5291	44.0134	48.5	4.455494	374.58	1.11	3.77	124.12	174.32

The normalized matrix is shown in table 37 using the MAUT method. While creating the normalized decision matrix, it is created by maximizing or minimizing. The alternatives are maximized or minimized according to the desired situation. Thus, the normalized decision matrix is obtained. It is shown in Equations 32 and 33.

Table 37. Normalised matrix for MAUT mehod

	C1	C2	C3	C4	C5	C6	C7	C8	C9	C10
A1	0.92941	0.72333	0.94920	0.00000	0.34797	0.527934	0	0.75000	0	1
A2	1.00000	1.00000	0.94730	0.25000	0.63794	0.697824	0.096774	0.70000	0.123606	0.947464
A3	1.02941	0.89833	1.00000	0.25000	0.84063	0.838852	0.16129	0.70000	0.22809	0.773805
A4	0.21176	-0.03917	0.20642	0.00000	0.10134	0.220751	0.258065	0.00000	0.086615	0.956585
A5	0.29412	0.15667	0.44090	0.25000	0.40601	0.840429	0.451613	0.35000	0.305827	0.916089
A6	0.33529	0.25000	0.51798	0.50000	0.66691	0.900662	0.677419	0.45000	0.405645	0.7417
A7	0.31765	0.23333	0.49950	0.50000	1.00000	0.963576	1	0.60000	0.515365	0.669829
A8	0.00000	-0.29083	0.00000	0.25000	0.00000	0	0.354839	-0.05000	0.464944	0.437796
A9	0.06471	-0.03417	0.12947	0.50000	0.47844	0.628508	0.645161	0.15000	0.724334	0.234221
A10	0.10000	0.07500	0.16534	1.00000	0.69617	0.83018	0.741935	0.45000	0.86672	0.145932
A11	0.07059	0.00000	0.16469	1.00000	0.78326	1	0.677419	1.00000	1	0

The weighted normalized matrix was obtained using the MAUT method. It is shown in Table 38.

Table 38. Weighted Normalized R Matrix

C1	C2	C3	C4	C5	C6	C7	C8	C9	C10
0.013081852	0.007423783	0.032613	0	0.007642	0.019253	0	0.033043	0	0.126255
0.016381396	0.018555515	0.032415	0.001094	0.02982	0.037577	0.000914	0.027672	0.002949	0.106832
0.017975247	0.013403531	0.038329	0.001094	0.060986	0.061164	0.002559	0.027672	0.010228	0.060245
0.000437283	0.000016579	0.000971	0	0.000613	0.002991	0.006686	0	0.001442	0.10999
0.000861475	0.000268348	0.004786	0.001094	0.01064	0.061485	0.021966	0.005703	0.018778	0.096592
0.001134417	0.000696508	0.006865	0.004817	0.033256	0.074905	0.056538	0.009823	0.034256	0.053894
0.001012195	0.000604273	0.006322	0.004817	0.102013	0.091679	0.166821	0.018964	0.058264	0.041607
0	0.000953208	0	0.001094	0	0	0.013028	0.00011	0.046218	0.015524
0.000040001	0.000012614	0.000377	0.004817	0.015272	0.029015	0.050121	0.000996	0.132126	0.004144
0.000095819	0.000060918	0.000618	0.029141	0.037024	0.059424	0.071269	0.009823	0.214411	0.001582
0.000047624	0	0.000613	0.029141	0.05028	0.102916	0.056538	0.075193	0.329073	0

Ranking is obtained using the MAUT method. It is shown in Table 39. In the final process, the alternatives are listed.

Table 39. Final Ranking for MAUT method

	Final Score	Rank
A1	0.2393117397	8
A2	0.2742086746	6
A3	0.2936545709	4
A4	0.1231477504	10
A5	0.2221735151	9
A6	0.2761847234	5
A7	0.4921020909	2
A8	0.0769260223	11
A9	0.2369208738	7
A10	0.4234498477	3
A11	0.6438020592	1

According to the results obtained: It can be seen from the table 18 that the best value can be obtained from the B20G90 fuel mixture. That is, good results are obtained from the mixture of 20% Biodiesel and 90 ppm graphene oxide

MOORA METHOD

The decision matrix is shown in table 40 by using the MOORA method.

Table 40. Decision matrix for MOORA method

	C1	C2	C3	C4	C5	C6	C7	C8	C9	C10
A1	0.0899	0.0900	0.0932	0.0893	0.0880	0.0931	0.1019	0.0938	0.1106	0.0849
A2	0.0898	0.0895	0.0932	0.0903	0.0923	0.0906	0.0996	0.0933	0.1049	0.0857
A3	0.0897	0.0897	0.0935	0.0903	0.0953	0.0885	0.0981	0.0933	0.1001	0.0885
A4	0.0913	0.0915	0.0897	0.0893	0.0844	0.0976	0.0958	0.0862	0.1066	0.0856
A5	0.0911	0.0911	0.0908	0.0903	0.0889	0.0885	0.0911	0.0897	0.0966	0.0862
A6	0.0910	0.0909	0.0912	0.0913	0.0928	0.0876	0.0857	0.0908	0.0920	0.0890
A7	0.0911	0.0910	0.0911	0.0913	0.0977	0.0867	0.0780	0.0923	0.0870	0.0901
A8	0.0916	0.0920	0.0888	0.0903	0.0829	0.1008	0.0934	0.0857	0.0893	0.0938
A9	0.0915	0.0915	0.0894	0.0913	0.0900	0.0916	0.0865	0.0877	0.0774	0.0970
A10	0.0915	0.0913	0.0895	0.0932	0.0932	0.0887	0.0842	0.0908	0.0709	0.0984
A11	0.0915	0.0914	0.0895	0.0932	0.0945	0.0862	0.0857	0.0964	0.0647	0.1007

The decision matrix obtained by using the MOORA method and equation 36 is shown in the normalized table 41.

Table 41. Normalized Matrix for MOORA method

	C1	C2	C3	C4	C5	C6	C7	C8	C9	C10
A1	0.445026	0.445471	0.452655	0.444341	0.438047	0.453825	0.468173	0.459501	0.476079	0.440494
A2	0.444376	0.442754	0.452611	0.449119	0.459465	0.441737	0.457533	0.456997	0.451689	0.444812
A3	0.444106	0.443752	0.453817	0.449119	0.474436	0.431703	0.45044	0.456997	0.431072	0.459084
A4	0.451628	0.452961	0.435656	0.444341	0.419831	0.475681	0.439799	0.42194	0.458988	0.444062
A5	0.450871	0.451037	0.441022	0.449119	0.442334	0.431591	0.418519	0.439469	0.415732	0.44739
A6	0.450492	0.450121	0.442786	0.453896	0.461604	0.427305	0.393691	0.444477	0.396036	0.461723
A7	0.450654	0.450284	0.442363	0.453896	0.486206	0.422829	0.358224	0.451989	0.374386	0.46763
A8	0.453577	0.455433	0.430932	0.449119	0.412346	0.491388	0.429159	0.419436	0.384335	0.486699
A9	0.452981	0.452912	0.433895	0.453896	0.447684	0.446669	0.397238	0.429452	0.333152	0.50343
A10	0.452656	0.45184	0.434716	0.463452	0.463765	0.43232	0.386598	0.444477	0.305056	0.510686
A11	0.452927	0.452576	0.434701	0.463452	0.470198	0.420237	0.393691	0.472022	0.278757	0.52268

The Weighted Normalized matrix was obtained using the MOORA method and equation 37 and is shown in table 42.

Table 42. Weighted Normalized matrix for MOORA method

	C1	C2	C3	C4	C5	C6	C7	C8	C9	C10
A1	0.007256	0.008227	0.017269	0.012888	0.044478	0.046489	0.077737	0.034391	0.155935	0.055356
A2	0.007246	0.008177	0.017267	0.013027	0.046653	0.04525	0.075971	0.034203	0.147946	0.055898
A3	0.007241	0.008196	0.017313	0.013027	0.048173	0.044222	0.074793	0.034203	0.141194	0.057692
A4	0.007364	0.008366	0.01662	0.012888	0.042629	0.048727	0.073026	0.031579	0.150337	0.055804
A5	0.007351	0.00833	0.016825	0.013027	0.044914	0.044211	0.069493	0.032891	0.136169	0.056222
A6	0.007345	0.008313	0.016892	0.013165	0.04687	0.043772	0.06537	0.033266	0.129718	0.058023
A7	0.007348	0.008316	0.016876	0.013165	0.049368	0.043313	0.059481	0.033828	0.122627	0.058766
A8	0.007396	0.008411	0.01644	0.013027	0.041869	0.050336	0.071259	0.031392	0.125885	0.061162
A9	0.007386	0.008365	0.016553	0.013165	0.045457	0.045755	0.065959	0.032142	0.109121	0.063265
A10	0.007381	0.008345	0.016584	0.013443	0.04709	0.044286	0.064192	0.033266	0.099918	0.064177
A11	0.007385	0.008359	0.016584	0.013443	0.047743	0.043048	0.06537	0.035328	0.091304	0.065684

Ranking is obtained using MOORA method and equation 38 and is shown in table 43.

Table 43. Ranks for MOORA method

		Rank
Y1	-0.2419745	11
Y2	-0.2293383	9
Y3	-0.2206212	7
Y4	-0.2399077	10
Y5	-0.2141201	6
Y6	-0.2023479	5
Y7	-0.1866127	3
Y8	-0.2217227	8
Y9	-0.1925338	4
Y10	-0.1779156	2
Y11	-0.1680528	1

According to the results obtained: It can be seen from the table 43 that the best value can be obtained from the B20G90 fuel mixture. That is, good results are obtained from the mixture of 20% Biodiesel and 90 ppm graphene oxide.

Inorder to make a decision 6 different MCDM method used and the ranks were tabulated in table 44.

Table 44. Ranks of the alternatives according to methods

Alternative	MAIRCA	TOPSIS	MOOSRA	COPRAS	MAUT	MOORA
A1	11	11	11	11	8	11
A2	9	9	10	9	6	9
A3	7	8	8	8	4	7
A4	10	10	9	10	10	10
A5	6	7	7	6	9	6
A6	5	6	6	5	5	5
A7	1	4	5	3	2	3
A8	8	5	4	7	11	8
A9	4	3	3	4	7	4
A10	3	2	2	2	3	2
A11	2	1	1	1	1	1

There are some differences in the ranks of the preferences so borda method was used to maket he decision more precise.

BORDA

Table 45. Results of Borda method

Alternative	Borda Number	The Ranks
A1	3	11
A2	14	9
A3	24	7
A4	7	10
A5	25	6
A6	34	5
A7	48	3
A8	23	8
A9	41	4
A10	52	2
A11	59	1

Once the borda number calculated the ranks are decided. Final rankings were tabulated in table 46.

Table 46 . Final Ranking of alternatives acording to Borda

Alternative	Borda Rank
A1	11
A2	9
A3	7
A4	10
A5	6
A6	5
A7	3
A8	8
A9	4
A10	2
A11	1

From the results obtained according to the BORDA method, it can be seen that the best option is A11. It can be seen from the table 46 that the best value can be obtained from the B20G90

fuel mixture. That is, good results are obtained from the mixture of 20% Biodiesel and 90 ppm graphene oxide.

Various criteria values of biodiesel graphene blended fuels at different ratios (30, 60, 90 ppm graphene, B0, B10, B20 biodiesel) taken from Hosseini's study are given. The density value, kinematic viscosity value, high temperature value and cetane number resulting from mixing the fuels at different ratios are given. At the same time, in the same study, the following values are obtained as a result of the combustion of these fuel mixtures; brake power, specific fuel consumption, emission values of gases such as CO, CO_2, UHC, NO_x are given. In our study, which of these fuels can be more alternative is optimized by using multi-criteria decision making methods. Multi-criteria decision making methods used are; Standard Deviation for weighing the criterion, TOPSIS, COPRAS, MAUT, MAIRCA, MOORA, MOOSRA and finally BORDA method. In the study, first of all, an alternative ranking from A1 to A11 is given to each of the fuel mixtures. Then, another process is carried out; each of the criteria such as CO, CO_2, NO_x; UHC, SFC, Brake Power, Density, Kinematic viscosity, Higher Heating Value etc. are ranked starting from C1 to C10. According to this ranking, the alternatives that emerged using the multi-criteria decision making method are ranked one by one and the best alternative is selected.

6. CONCLUSION

The quest for sustainable energy sources has been a pressing global concern for decades, driven by the need to mitigate climate change and reduce environmental degradation. Since the Industrial Revolution, reliance on fossil fuels such as coal, oil, and natural gas has been the cornerstone of modern civilization's energy consumption. However, the combustion of these fossil fuels releases significant quantities of greenhouse gases (GHGs), primarily carbon dioxide (CO_2), methane (CH_4), and nitrous oxide (N_2O), into the atmosphere, contributing to global warming and climate change. Energy is one of the most important needs for people today. With the introduction of fossil fuels into the market and the revelation of their damages, energy production has been directed towards new and more environmentally friendly fuel sources. One of these sources is graphene and graphene oxide, which consist of nanoparticles. Studies on these innovative graphene and graphene oxide-enhanced fuels are promising. In this study, seven different MCDM (Multi-Criteria Decision Making) methods were used to determine the optimal fuel blend mixed with various graphene ratios. The purpose of this study is to determine the most suitable alternative fuel mixture using the multi-criteria decision-making method. The most suitable and most accurate approach to the different multi-criteria decision-making methods used is determined and that method is used. Thus, the most systematic approach is found and the risk formation is reduced. Using these methods, the most suitable fuel mixture is found depending on the given criteria.

The research design provides a systematic approach to investigate the impacts of graphene-doped fuel blends on greenhouse gas emissions. By employing a structured framework and rigorous methodology, this study aims to generate reliable and comprehensive insights into the environmental and technical benefits of using graphene-doped fuel blends. The integration of MCDM methods ensures a balanced evaluation of multiple criteria, facilitating informed decision-making in the context of sustainable fuel development. According to the multi-criteria decision making method, the best alternative was determined by the TOPSIS method, COPRAS method, MOOSRA method, MAUT Method and MOORA method A11 (which is B20G90), while with the MAIRCA method A7 (which is B10G90) was determined.The final decision from the results obtained using the six different MCDM methods was made using the Borda method. With the BORDA method, multi-criteria decision-making methods results were ranked and a scoring system was created. Therefore, the best blend among them was selected. From the results obtained according to the BORDA method, it can be seen that the

best option is A11 which is B20G90. That is, good results are obtained from the mixture of 20% Biodiesel and 90 ppm graphene oxide. Accordingly, the most suitable density value for B20G90 is: 0.8369 g/cm^3. The best kinematic viscosity value: 5.5291 mm^2/s, higher heating value: 44.0134 Mj/kg, cetane number: 48.5, brake power: 4.4554, specific fuel consumption SFC 374.58, for CO 1.11, CO_2 3.77, UHC 124.12 and NOx 174.32, respectively. As can be seen, using these methods will make it easier to choose the best blend if there are multiple alternatives.

7. REFERENCES

Wang, W., Wang, Y., Gao, Y., & Zhao, Y. (2014). Control of number of graphene layers using ultrasound in supercritical CO2 and their application in lithium-ion batteries. *The journal of supercritical fluids*, *85*, 95-101.

Elbasuney, S., Yehia, M., Ismael, S., Al-Hazmi, N. E., El-Sayyad, G. S., & Tantawy, H. (2023). Potential impact of reduced graphene oxide incorporated metal oxide nanocomposites as antimicrobial, and antibiofilm agents against pathogenic microbes: Bacterial protein leakage reaction mechanism. *Journal of Cluster Science*, *34*(2), 823-840.

Mousavi, S. M., Low, F. W., Hashemi, S. A., Lai, C. W., Ghasemi, Y., Soroshnia, S., & Tiong, S. K. (2020). Development of graphene based nanocomposites towards medical and biological applications. *Artificial cells, nanomedicine, and biotechnology*, *48*(1), 1189-1205.

Sajeevan, A. C., & Sajith, V., (2013)"Diesel engine emission reduction using catalytic nanoparticles: an experimental investigation", Journal of Engineering.75,90-100.

Karthikeyan S., & Prathima A., (2017) "Microalgae biofuel with CeO2 nano additives as an ecofriendly fuel for CI engine", Energy Sources, Part A: Recovery, Utilization, and Environmental Effects,39:13, 1332-1338

Ranaware, A. A., & Satpue S.T.,(2013) "Correlation between Effects of Cerium Oxide Nanoparticles and Ferrofluid on the Performance and Emission Characteristics of a C.I. Engine", Journal of Mechanical and Civil Engineering, 55-59.

Vellaıyan S.,(2020)"Effect of cerıum oxıde nanoadditive on the workıng characterıstıcs of water emulsıfıed bıodıesel fueled dıesel engıne: an experimental study", Thermal Science, 24(1A), 231-241.

An, H., Maghbouli, A., Li, J., Chou, S.K., & Chua, K.J.,(2013) "Performance, combustion and emission characteristics of biodiesel derived from waste cooking oils", Applied Energy, 112,493-499.

Muralidharan K., & Vasudevan D.,(2011) "Performance, emission and combustion characteristics of a variable compression ratio engine using methyl esters of waste cooking oil and diesel blends" Applied Energy, 88,3959-3968.Chen, Z., Liu, Y., & Luo, J. (2016). Tribological properties of few-layer graphene oxide sheets as oil-based lubricant additives. *Chinese Journal of Mechanical Engineering*, *29*(2), 439-444

Heidari-Maleni, A., Gundoshmian, T. M., Jahanbakhshi, A., & Ghobadian, B. (2020). Performance improvement and exhaust emissions reduction in diesel engine through the use of graphene quantum dot (GQD) nanoparticles and ethanol-biodiesel blends. *Fuel*, *267*, 117116.

Agharkar, M., Kochrekar, S., Hidouri, S., & Azeez, M. A. (2014). Trends in green reduction of graphene oxides, issues and challenges: a review. *Materials Research Bulletin*, *59*, 323-328.

Phiri, J., Gane, P., & Maloney, T. C. (2017). General overview of graphene: Production, properties and application in polymer composites. *Materials Science and Engineering: B*, *215*, 9-28.

Nag, A., Mitra, A., & Mukhopadhyay, S. C. (2018). Graphene and its sensor-based applications: A review. *Sensors and Actuators A: physical*, *270*, 177-194.

Hoseini, S. S., Najafi, G., Ghobadian, B., Ebadi, M. T., Mamat, R., & Yusaf, T. J. R. E. (2020). Biodiesels from three feedstock: The effect of graphene oxide (GO) nanoparticles diesel engine parameters fuelled with biodiesel. *Renewable energy*, *145*, 190-201.

Rajpoot, A. S., Choudhary, T., Chelladurai, H., & Patel, N. K. (2023). Effect of graphene nanoparticles on the behavior of a CI engine fueled with Jatropha biodiesel. *Materials Today: Proceedings*.

Jana, M. Saha, S. Khanra, P. Murmu, N.C. Srivastava, S.K. Kuila, T. and Lee, J.H., (2014). Bio-reduction of graphene oxide using drained water from soaked mung beans (Phaseolus aureus L.) and its application as energy storage electrode material", Materials Science and Engineering: B, 186, 33-40

Haghighi, B., & Tabrizi, M. A. (2013). Green-synthesis of reduced graphene oxide nanosheets using rose water and a survey on their characteristics and applications. *RSC advances*, *3*(32), 13365-13371.

Gurunathan, S., Han, J. W., Park, J. H., Eppakayala, V., & Kim, J. H. (2014). Ginkgo biloba: a natural reducing agent for the synthesis of cytocompatible graphene. *International journal of nanomedicine*, 363-377.

Suresh, D., Kumar, M. P., Nagabhushana, H., & Sharma, S. C. (2015). Cinnamon supported facile green reduction of graphene oxide, its dye elimination and antioxidant activities. *Materials Letters*, *151*, 93-95.

Kuila, T., Bose, S., Khanra, P., Mishra, A. K., Kim, N. H., & Lee, J. H. (2012). A green approach for the reduction of graphene oxide by wild carrot root. *Carbon*, *50*(3), 914-921.

Hettiarachchi, S. J., Bowen, J., Kershaw, M., Baragau, I. A., Nicolaev, A., & Kellici, S. (2023). Nanostructured Al2O3/graphene additive in bio-based lubricant: A novel approach to improve engine performance. *Tribology International*, *186*, 108619.

Jiang, Y., Demko, A. R., Baek, J., Shi, X., Vallez, L., Ning, R., & Zheng, X. (2020). Facilitating laser ignition and combustion of boron with a mixture of graphene oxide and graphite fluoride. *Applications in Energy and Combustion Science*, *1*, 100013.

Sharma, V., Hossain, A. K., Ahmed, A., & Rezk, A. (2022). Study on using graphene and graphite nanoparticles as fuel additives in waste cooking oil biodiesel. *Fuel*, *328*, 125270.

Soudagar, M. E. M., Nik-Ghazali, N. N., Kalam, M. A., Badruddin, I. A., Banapurmath, N., Khan, T. Y., ... & Afzal, A. (2019). The effects of graphene oxide nanoparticle additive stably dispersed in dairy scum oil biodiesel-diesel fuel blend on CI engine: performance, emission and combustion characteristics. *Fuel*, *257*, 116015.

Gowtham, M., & Prakash, R. (2020). Control of regulated and unregulated emissions from a CI engine using reformulated nano fuel emulsions. *Fuel*, *271*, 117596.

Gundoshmian, T. M., Heidari-Maleni, A., & Jahanbakhshi, A. (2021). Evaluation of performance and emission characteristics of a CI engine using functional multi-walled carbon nanotubes (MWCNTs-COOH) additives in biodiesel-diesel blends. *Fuel*, *287*, 119525.

Anbarsooz, M. (2023). Combustion characteristics of nanofuels: A comprehensive review on diesel/biodiesel-based nanofuels. *Fuel*, *337*, 126834.

Gad, M. S., Ağbulut, Ü., Afzal, A., Panchal, H., Jayaraj, S., Qasem, N. A., & El-Shafay, A. S. (2023). A comprehensive review on the usage of the nano-sized particles along with diesel/biofuel blends and their impacts on engine behaviors. *Fuel*, *339*, 127364.

Atelge, M. R., Arslan, E., Kahraman, N., & Ünalan, S. (2023). Evaluation of hybrid nanoparticles to oxygenated fuel with ethanol and n-butanol on combustion behavior. *Fuel*, *344*, 128048.

Küçükosman, R., Yontar, A. A., & Ocakoglu, K. (2022). Nanoparticle additive fuels: Atomization, combustion and fuel characteristics. *Journal of Analytical and Applied Pyrolysis*, *165*, 105575.

EL-Seesy, A. I., Hassan, H., & Ookawara, S. J. E. C. (2018). Performance, combustion, and emission characteristics of a diesel engine fueled with Jatropha methyl ester and graphene oxide additives. *Energy conversion and management*, *166*, 674-686.

Bayindirli, C., Celik, M., & Zan, R. (2023). Optimizing the thermophysical properties and combustion performance of biodiesel by graphite and reduced graphene oxide nanoparticle fuel additive. *Engineering Science and Technology, an International Journal*, *37*, 101295.

Razzaq, L., Mujtaba, M. A., Soudagar, M. E. M., Ahmed, W., Fayaz, H., Bashir, S., ... & El-Seesy, A. I. (2021). Engine performance and emission characteristics of palm biodiesel blends with graphene oxide nanoplatelets and dimethyl carbonate additives. *Journal of environmental management*, *282*, 111917.

Ağbulut, Ü., Elibol, E., Demirci, T., Sarıdemir, S., Gürel, A. E., Rajak, U., ... & Verma, T. N. (2022). Synthesis of graphene oxide nanoparticles and the influences of their usage as fuel additives on CI engine behaviors. *Energy*, *244*, 122603.

Chacko, N., & Jeyaseelan, T. (2020). Comparative evaluation of graphene oxide and graphene nanoplatelets as fuel additives on the combustion and emission characteristics of a diesel engine fuelled with diesel and biodiesel blend. *Fuel Processing Technology*, *204*, 106406.

El-Seesy, A. I., & Hassan, H. (2019). Investigation of the effect of adding graphene oxide, graphene nanoplatelet, and multiwalled carbon nanotube additives with n-butanol-Jatropha methyl ester on a diesel engine performance. *Renewable Energy*, *132*, 558-574.

Hoseini, S. S., Najafi, G., Ghobadian, B., Ebadi, M. T., Mamat, R., & Yusaf, T. J. R. E. (2020). Performance and emission characteristics of a CI engine using graphene oxide (GO) nano-particles additives in biodiesel-diesel blends. *Renewable Energy*, *145*, 458-465.

Can, Ö., & Çetin, Ö. (2023). Potential use of graphene oxide as an engine oil additive for energy savings in a diesel engine. *Engineering Science and Technology, an International Journal*, *48*, 101567.

Pireh, M. E., Parashkoohi, M. G., & Zamani, D. M. (2022). Evaluation of combustion characteristics performances and emissions of a diesel engine using diesel and biodiesel fuel blends containing graphene oxide nanoparticles. *Open Agriculture*, *7*(1), 935-947.

Murugan, N., Venu, H., Jayaraman, J., & Appavu, P. (2022). Emission and performance characteristics study on nanographene oxide additives doped palm oil methyl ester blend in a diesel engine. *International Journal of Ambient Energy*, *43*(1), 1304-1310.

Abdulvahitoglu, A., Kilic, M., 2022. A new approach for selecting the most suitable oilseed for biodiesel production; the integrated AHP-TOPSIS method. Ain Shams Eng. J. 13, 101604. https://doi.org/10.1016/j.asej.2021.10.002

Abdulvahitoğlu, A., Macit, İ., Koyuncu, M., 2021. Jandarma karakolu kuruluş yerinin AHP-TOPSIS tabanlı bir matematiksel model ile seçimi ve CAS/CBS ile analizi, Güvenlik Bilimleri Dergisi. https://doi.org/10.28956/gbd1028022

Abdulvahitoğlu, A., Abdulvahitoğlu, A., 2022. Elektrikli Araç Bataryalarının Bütünleşik Swara -Topsis Metodu ile Değerlendirilmesi Assessment o f Electrıc Veh icle Batteries Via Integrated Swara-Topsis Approach Abstract 37, 1061–1076.

Abdulvahitoğlu, Adnan, Vural, D., Abdulvahitoğlu, Aslı, 2023. Optimising Traffic Safety – Locating Traffic Gendarmes Based on Multi-Criteria Decision Making. Promet - Traffic Transp. 35, 800–813. https://doi.org/10.7307/ptt.v35i6.318

Demir, G., 2021. Türk Çimento Firmalarının Finansal Performansının Bulanık SWARA - COPRAS- MAUT Yöntemleri ile Karşılaştırılması Comparison of the Financial Performance of Turkish Cement Firms with Fuzzy SWARA-COPRAS- 20, 1875–1892.

Demir, G., Özyalçın, A.T., Bircan, H., 2021. Çok Kriterli Karar Verme Yöntemleri ve ÇKKV Yazılımı ile Problem Çözümü. Nobel Yayınevi, Ankara.

Taherdoost, H., Madanchian, M., 2023. Multi-Criteria Decision Making (MCDM) Methods and Concepts. Encyclopedia 3, 77–87. https://doi.org/10.3390/encyclopedia3010006

DeLuchi, M. A., Johnston, R. A., & Sperling, D. (1987). Transportation Fuels and the Greenhouse Effect Universitywide Energy Research Group. University of California, California.

Qu, L., Liu, Y., Baek, J. B., & Dai, L. (2010). Nitrogen-doped graphene as efficient metal-free electrocatalyst for oxygen reduction in fuel cells. ACS nano, 4(3), 1321-1326.

Shown, I., Hsu, H. C., Chang, Y. C., Lin, C. H., Roy, P. K., Ganguly, A., ... & Chen, K. H. (2014). Highly efficient visible light photocatalytic reduction of CO2 to hydrocarbon fuels by Cu-nanoparticle decorated graphene oxide. Nano letters, 14(11), 6097-6103.

Najafabadi, A. T. (2015). Emerging applications of graphene and its derivatives in carbon capture and conversion: Current status and future prospects. Renewable and Sustainable Energy Reviews, 41, 1515-1545.

Haque, E., Sarkar, S., Hassan, M., Hossain, M. S., Minett, A. I., Dou, S. X., & Gomes, V. G. (2016). Tuning graphene for energy and environmental applications: Oxygen reduction reaction and greenhouse gas mitigation. Journal of Power Sources, 328, 472-481.

Ooi, J. B., Ismail, H. M., Swamy, V., Wang, X., Swain, A. K., & Rajanren, J. R. (2016). Graphite oxide nanoparticle as a diesel fuel additive for cleaner emissions and lower fuel consumption. Energy & Fuels, 30(2), 1341-1353.

Hoseini, S. S., Najafi, G., Ghobadian, B., Mamat, R., Ebadi, M. T., & Yusaf, T. (2018). Novel environmentally friendly fuel: The effects of nanographene oxide additives on the performance and emission characteristics of diesel engines fuelled with Ailanthus altissima biodiesel. Renewable energy, 125, 283-294.

Feng, L., Qin, Z., Huang, Y., Peng, K., Wang, F., Yan, Y., & Chen, Y. (2020). Boron-, sulfur-, and phosphorus-doped graphene for environmental applications. Science of The Total Environment, 698, 134239.

Hoseini, S. S., Najafi, G., Ghobadian, B., Ebadi, M. T., Mamat, R., & Yusaf, T. J. R. E. (2020). Performance and emission characteristics of a CI engine using graphene oxide (GO) nano-particles additives in biodiesel-diesel blends. Renewable Energy, 145, 458-465.

Nair, J., Prasad Kumar, P., Thakur, A. K., Samhita, S., & Aravinda, A. (2021, February). Influence on emissions and performance of CI engine with graphene nanoparticles blended with Karanja biodiesel. In AIP Conference Proceedings (Vol. 2317, No. 1). AIP Publishing.

Ahmed, A., Shah, A. N., Azam, A., Uddin, G. M., Ali, M. S., Hassan, S., ... & Aslam, T. (2020). Environment-friendly novel fuel additives: Investigation of the effects of graphite nanoparticles

on performance and regulated gaseous emissions of CI engine. Energy conversion and management, 211, 112748.

Heidari-Maleni, A., Mesri-Gundoshmian, T., Jahanbakhshi, A., Karimi, B., & Ghobadian, B. (2021). Novel environmentally friendly fuel: The effect of adding graphene quantum dot (GQD) nanoparticles with ethanol-biodiesel blends on the performance and emission characteristics of a diesel engine. NanoImpact, 21, 100294.

Bidir, M. G., Narayanan Kalamegam, M., Adaramola, M. S., Hagos, F. Y., & Chandra Singh, R. (2023). Investigation of combustion, performance, and emissions of biodiesel blends using graphene nanoparticle as an additive. International Journal of Engine Research, 24(11), 4459-4469.

Performance of hybrid nano-PCM composite: Insights from T-history method and numerical analysis V. Krishna Raj ,V. Baiju , A. Asif Sha , K.L. Priya, S.B. Vishnu Journal of Energy Storage 90 (2024) 11170

V. Kavimani, K. Soorya Prakash, Titus Thankachan Multi-objective optimization in WEDM process of graphene – SiC-magnesium composite through hybrid techniques Measurement 145 (2019) 335–349

V. Anandan, M. Naresh Babu, M. Vetrivel Sezhian, Cagri Vakkas Yildirim, M. Dinesh Babu Journal of Manufacturing Processes 68 (2021) 90–103

Juan Xu, Xin Li, Ruofan Wang, Wentao Xue Cooperative communication and relay node selection algorithm based on SWIPT Physical Communication 64 (2024) 102332

Pankaj P. Awate, Shivprakash B. Barve Graphene/Al6061 nanocomposite selection using TOPSIS and EXPROM2 multi-criteria decision-making methods Selection and peer-review under responsibility of the scientific committee of the International Conference on Materials, Mechanics, Mechatronics and Manufacturing. Materials Today: Proceedings 62 (2022) 6425–6431

Khan, F., Karimi, M. N., Khan, O., Yadav, A. K., Alhodaib, A., Gürel, A. E., & Ağbulut, Ü. (2024). A hybrid MCDM optimization for utilization of novel set of biosynthesized nanofluids on thermal performance for solar thermal collectors. International Journal of Thermofluids, 22, 100686.

Ankur Dwivedi , Anoop Kumar, Varun Goel A consolidated decision-making framework for nano-additives selection in battery thermal manageme

Aslı Abdulvahitoglu, Kadir Aydin Performance and Exhaust Emission Characteristics of a CI Engine Fueled with Synthesized Fuel Blends (2012), Energy Education Science and Technology, Part A enegy Science and Research, 28(2) 699-710

VAN BASSHUYSEN R., and SCHÄFER F, “Internal combustion engine handbook : basics, components, systems, and perspectives”, SAE International and Professional Engineering Publishing ISBN: 978-0-7680-1139-5, Pages 629-634 , 2004

Aslı Abdulvahitoglu. Performance and Exhaust Emission Characteristics of a CI Engine Fueled with Synthesized Fuel Blends Çukurova Unıversıty Instıtue Of Natural And Applıed Scıences Department Of Mechanıcal Engıneerıng Adana, 2009, PhD Thesıs

Yu, Feng & Yin, Lianqian & Wang, Guizhou. (2023). A Worldwide Assessment of Quantitative Finance Research through Bibliometric Analysis. Applied Economics and Finance. 10. 1-17. 10.11114/aef.v10i2.5949.

Strong, C., Erickson, C., & Shukla, D. (2004). Evaluation of biodiesel Fuel: Literature review.